1961

The directional distribution of ambient noise in the ocean.

Becken, Bradford Albert

University of California, Los Angeles

THE DIRECTIONAL DISTRIBUTION OF AMBIENT NOISE IN THE OCEAN

BRADFORD ALBERT BECKEN

UNIVERSITY OF CALIFORNIA, LOS ANGELES

The Directional Distribution of Ambient Noise in the Ocean

A dissertation submitted in partial satisfaction of the requirements for the degree Doctor of Philosophy in Physics

by

Bradford Albert Becken

January 1961

TABLE OF CONTENTS

Chapter | Page

LIST OF FIGURES

Figure	Title	Page
24	True Field Distribution Iterative Solution . . .	81
25	$G(\theta)\,X(\theta)\sin\theta$ vs θ	83

I. INTRODUCTION

1.1 Background

Although extensive ocean ambient noise studies were conducted during World War II with continuing effort since that date, few of either theoretical or experimental treatments have dealt with the directional properties of such noise. There are many possible sources of ambient noise in the ocean any of which could produce non-uniform distributions. R. A. Frosch[1] in examining likely contributors to the total acoustic energy content of the oceans has considered, for example, biological sources, seismic noise, shipping, lightning and sea surface waves. His conclusion that sea surface waves are a major contributor is in agreement with World War II data. For example, the "Knudsen"[2] curves, a compilation of omni-directional measurements relating ambient noise spectrum levels to frequency as a function of sea state, exhibit a direct sea state/ambient noise interdependence and by their very nature permit the inference of noise anisotropy in the ocean.

Theoretical treatments considering the ocean surface as a possible noise source have been published by Eckart[3], Roberson[4], Urick[5] and Miller[6]. Eckart has presented the physical picture of the ocean surface resolved into sinusoidal travelling waves of the particular phase velocity which would be associated with free flexural waves of an elastic plate excited by random local shocks of short duration. The above model would result in the generation of sound only under the unlikely condition that the surface phase velocity exceeded the velocity of the bounded medium. Roberson

without attention to a physical model of noise production considered both an infinite volume distribution of simple sources and the combined effect of a volume distribution of simple sources bounded by a surface distribution of dipole sources. Assuming an attenuation law proportional to frequency squared, he showed a -6 decibel/octave dependence of noise upon frequency for the unbounded case and a nonuniform dependence upon frequency for the mixed case depending upon the ratio of the contributions from the two sources and the frequency. In this latter case, no combination of surface and volume sources produced a constant slope in agreement with the "Knudsen" curves except over a limited frequency range.

Urick specifically considered the subject of directional distribution of ambient noise and concluded that significant anisotropy might exist depending upon the unknown manner in which each element of surface radiates.

Miller considered the directional distribution resulting from the combination of straight path propagation from surface radiators close to the receiver and convergent zone propagation from distant surface radiators. The acoustic radiation from the surface varied as cosine θ, where θ is the angle between the direction of radiation and a normal to the radiating surface. No bottom reflection or volume sources were assumed. He concluded, tentatively, that noise in the above case is essentially isotropic over a hemisphere with a slight increase within $\pm$ 9 degrees of the horizontal and that the area immediately above and close to the receiver

contributes about the same total noise as the contribution from the first convergence zone.

If the ocean surface is a major contributor to ambient noise, it has been reasoned that ambient level should decrease with depth. The change in ambient noise levels with depth[7] has been investigated experimentally. No such change has been detected to depths of 300 feet in tests at 25 kilocycles per second. Urick[5] has shown, however, that the change to be expected between 3 and 300 feet depth, even at a higher frequency of 50 kilocycles per second where attenuation is greater, is only 3 decibels theoretically and thus a smaller change would have been obscured by measurement fluctuations at the lower frequencies. Teer[8] reported the results of tests at 19 kilocycles per second with a small line array oriented horizontally and vertically in deep water. The results, which seemed to indicate that ambient noise is isotropic, are not considered conclusive because of limitations in equipment and the environmental conditions experienced during the tests.

In summary, no experimental data exist to describe the directional distribution of ocean ambient noise. Theoretical treatments have indicated either isotropic or anisotropic distributions may exist depending upon initial assumptions as to the nature of the surface radiator and the uncertain effect of ocean sound channels.

1.2 Research Objectives

It is the purpose of this study to investigate anisotropy of deep ocean ambient noise in the frequency range of 750 to 1500

cycles per second. Further specific objectives will be:

a. To isolate vertical and azimuthal dependencies.

b. To establish the identity of the sources contributing to non-uniform distributions.

c. To infer the radiation patterns of such sources.

II. AMBIENT NOISE EQUIPMENT

2.1 Discussion

There are two major reasons which have prevented more widespread investigation of the directional properties of ambient noise. The first concerns the limitation of a single directional hydrophone which, to monitor several directions in space successively, requires the assumption of a stationary process. The above difficulty may be overcome by the employment of more than one directional hydrophone or by forming several directional beams from an array of fixed non-directional hydrophone elements. Either solution generates a second problem, namely the difficulty of ensuring uniform gain in the several beams. Both limitations have been surmounted by a system conceived by Anderson[9] and implemented by the staff of the Marine Physical Laboratory of the Scripps Institution of Oceanography, University of California, La Jolla. A 32-element array has been constructed in the shape of a great stellated icosohedron as shown in Fig. 1. A summary of the array design parameters is contained in paragraph 2.2 following. The 32 hydrophone outputs are combined to form 32 beams with axes coinciding with lines passing through the array center and the individual hydrophones. All 32 hydrophones are used in forming each beam.

The problem of uniform sensitivity in each beam is minimized by employing clipped processing. At the output of each hydrophone channel prior to beam formation, all amplitude information is discarded by infinite clipping and phase information only retained. The clipped "on-off" form of the channel outputs permits digital

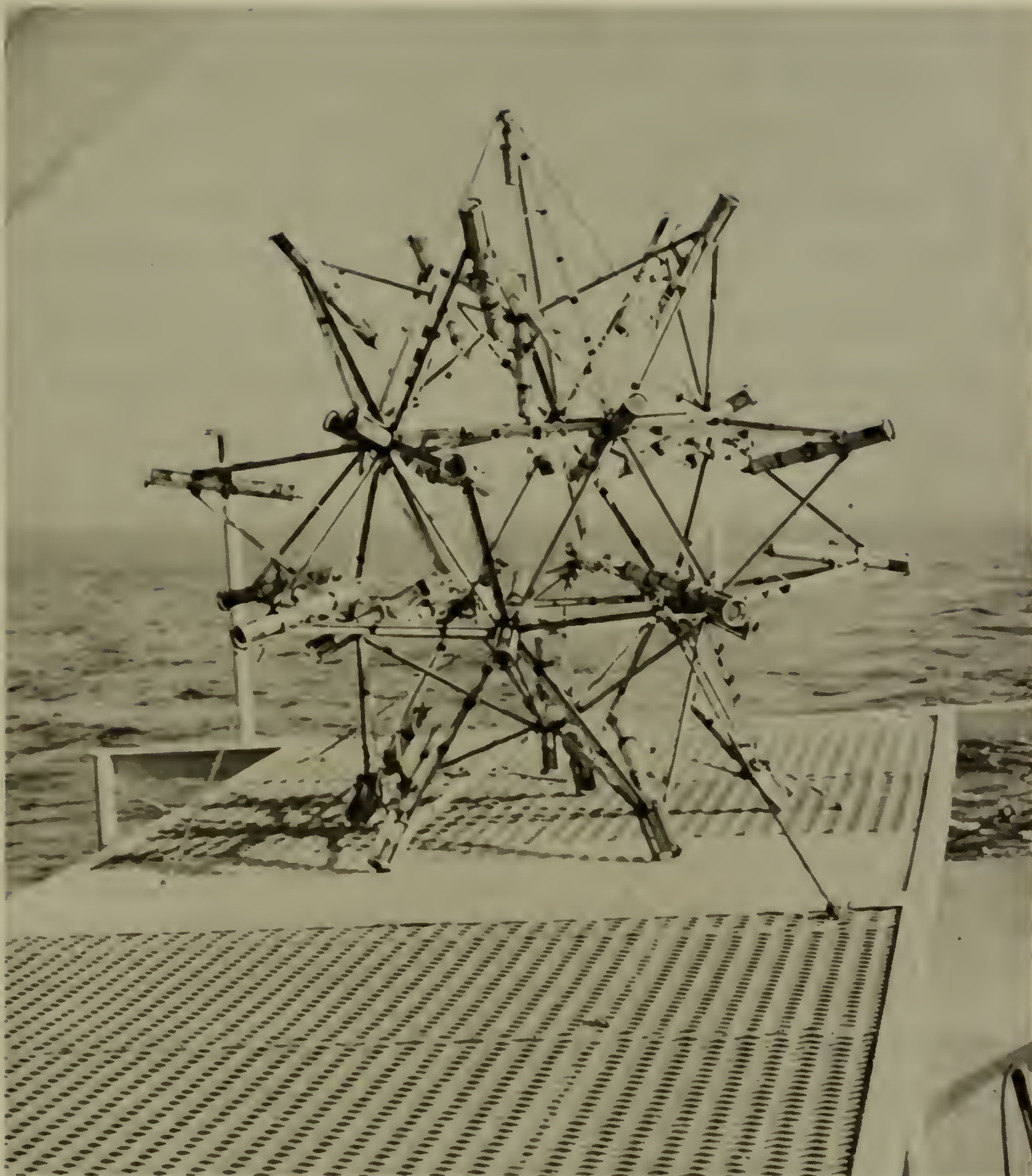

FIGURE 1. THE AMBIENT NOISE ARRAY

shift register techniques to be employed in the forming of the 32 beams with an attendant saving in space and equipment complexity over conventional analog beam forming techniques. The system is thus independent of individual channel gain differences from each hydrophone through the beam forming process. The problem of amplitude differences appears only in compensating for detector gain differences in the process of rectifying each beam output. The clipping and beam forming processes utilized in this system have been reported by Anderson[10] and Rudnick[11]. The restoration of the analog form of a signal from clipped hydrophone outputs is considered briefly in paragraph 2.5.

2.2 Array Configuration Development

In arriving at the present array geometry of a great stellated icosohedron, Anderson[9] considered three factors:

a. The number of elements.

b. Element configuration.

c. Element spacing.

Since presumably small deviations from an isotropic field were to be measured, a symmetrical distribution was suggested permitting nearly identical directivity patterns of the several beams to be formed by electrical steering. A distribution of elements in depth rather than a spherical shell would permit greater interelement spacings for a given array diameter and thus increased array efficiency through minimizing interelement correlations. The number of elements was limited by considerations of electronic complexity. Thirty-two

appeared a practical number and (a) and (b) above were satisfied by the great stellated icosohedron. Optimum design of interelement spacing was determined by calculations of array efficiency defined as the ratio of output to input signal to noise ratios. Signal in this case was the deviation from isotropy which it was desired to measure in a given direction. An interelement spacing of 0.6 wave lengths at the 1 kilocycle per second nominal center frequency was chosen.

2.3 General System Description

An overall system block diagram is shown in Fig. 2. For simplicity only 1 of 32 identical receiving channels is represented completely. Reading from the left, an individual hydrophone output is first amplified and then employed to frequency modulate a telemetering transmitter. The 32 transmitter carriers are distributed from 10 through 16.2 megacycles per second in 200 kilocycles per second increments. An additional 1 megacycle per second amplitude modulated transmitter relays hydrophone array azimuthal orientation in accordance with the directional indication of a magnetic compass. The 32 hydrophones, preamplifiers, telemetering transmitters and compass system comprise the underwater portion of the system.

The transmitter outputs are coupled to the shipborne receiving portion by coaxial cable. A 1500 foot length was available. The 3/8 inch diameter, doubly armored cable serves also as the supporting member of the 700 pound receiving array. Cable attenuations of 1.5 and 1.8 decibels per 100 feet at 10 and 16 megacycles

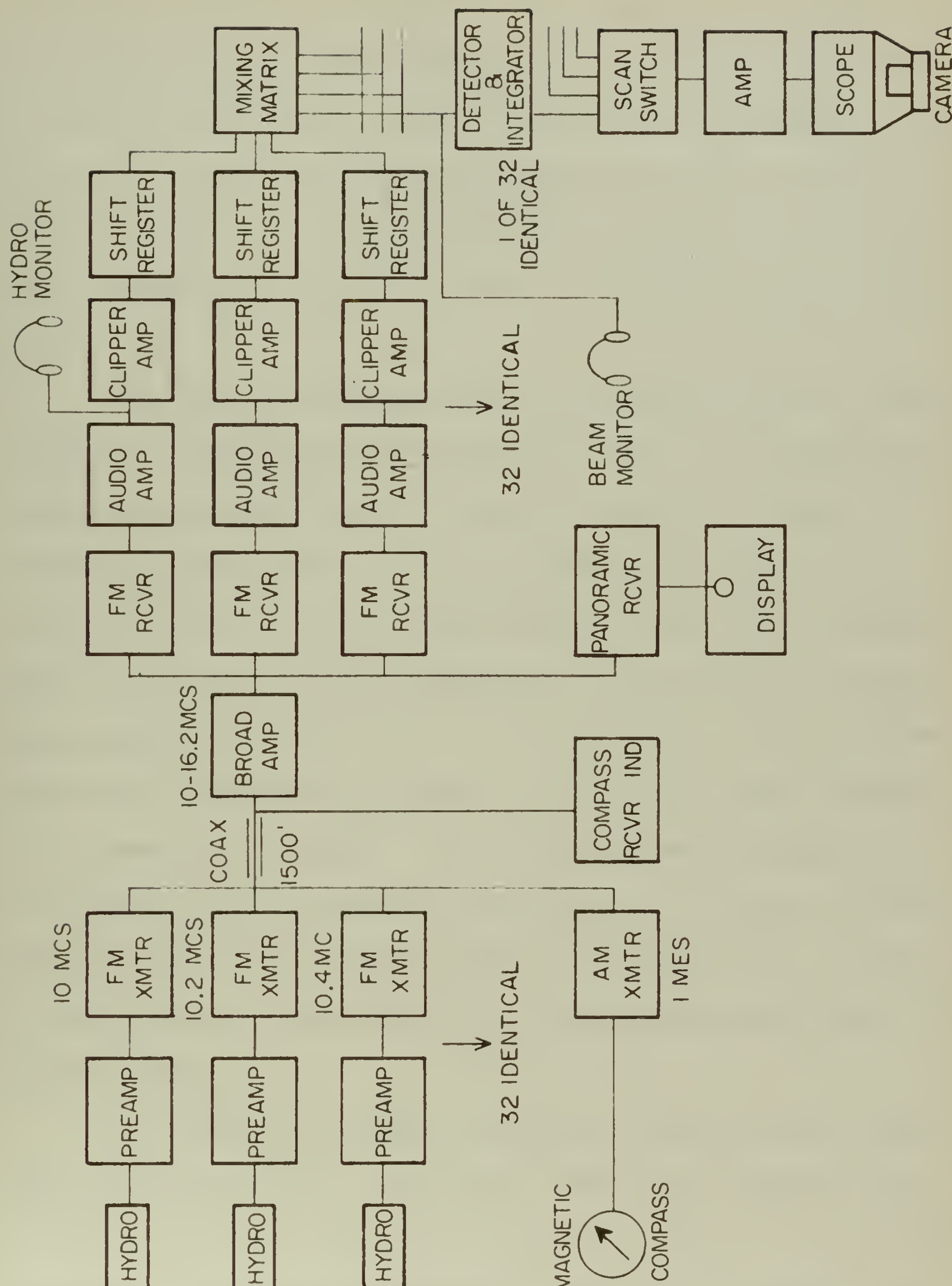

FIGURE 2. AMBIENT NOISE EQUIPMENT BLOCK DIAGRAM

per second respectively necessitated the insertion of a broadband 10 to 16.2 megacycle per second preamplifier prior to demodulation of the signal by the 32 matching frequency modulated receivers. At this stage it is possible to view the amplitude and spacing of the 32 individual carriers as well as the frequency deviation imposed by each signal by means of a panoramic receiver and cathode ray tube indicator.

Following demodulation in the FM receivers, the audio signal is further amplified and then infinitely clipped. All amplitude information is discarded and only polarity information retained. The clipped signal then enters a digital shift register ten bit delay line which provides suitable signal delay increments such that subsequent combination of the 32 signals in a mixing matrix yields 32 beams symmetrically spaced over $4\pi\Omega$. The 32 beam outputs are then individually detected and integrated by a simple low pass RC filter of one second time constant. Following detection and integration, the 32 beam outputs are sequentially sampled at a 30 cycle per second rate by a mercury jet scanning switch for presentation on a cathode ray oscilloscope. Sixteen millimeter scope photographs preserve the data for analysis.

All receiving equipment is housed in a portable Army Signal Corps communications hut. The entire 7,000 pound installation may be moved quickly by crane from its laboratory position to the fantail of PAOLINA T, a Scripps Institution of Oceanography research vessel. The electronic hut, array, associated winches and boom and gasoline powered 15 KW generator satisfying the 115 volt, 50 ampere demand

are shown in Figs. 3 and 4.

2.4 Hydrophone and Transmitter Assembly

The hydrophones are encapsulated barium titanate cylinders with a flat response averaging 90 decibels below 1 volt/μ bar throughout the range of interest, 750-1500 cycles per second. The cylindrical sensitive element is 1-1/2 inches high, 1-7/16 inches in diameter and has a wall thickness of 1/8 inch. Individual hydrophone directivity is discussed in paragraph 3.3. Although the particular units employed were constructed at the Marine Physical Laboratory, an identical unit, the REMACO Model R-130 is commercially available. They are rated at a working pressure in excess of 1600 pounds per square inch. The hydrophone fits into the end of a 16-1/2 inch long, 5/32 inch thick stainless steel pipe which forms the watertight housing for preamplifier and transmitter. All hydrophone units are series connected, 50 VDC required by each unit or 1600 VDC total. A relay feature is included to remove a particular hydrophone unit should a vacuum tube filament open. Were this feature not included the entire array would become disabled by the failure of a single tube. On the other hand, a short circuit anywhere in the series string disables all units beyond the point of shorting. A partially disassembled unit is shown in Fig. 5.

2.5 Clipped Processing

Because digital multibeam steering (DIMUS) is a relatively new technique, the following simplified illustration of the restoration of the analog form of a signal by the addition of several

[illegible]

[illegible]

[illegible]

[illegible]

[illegible]

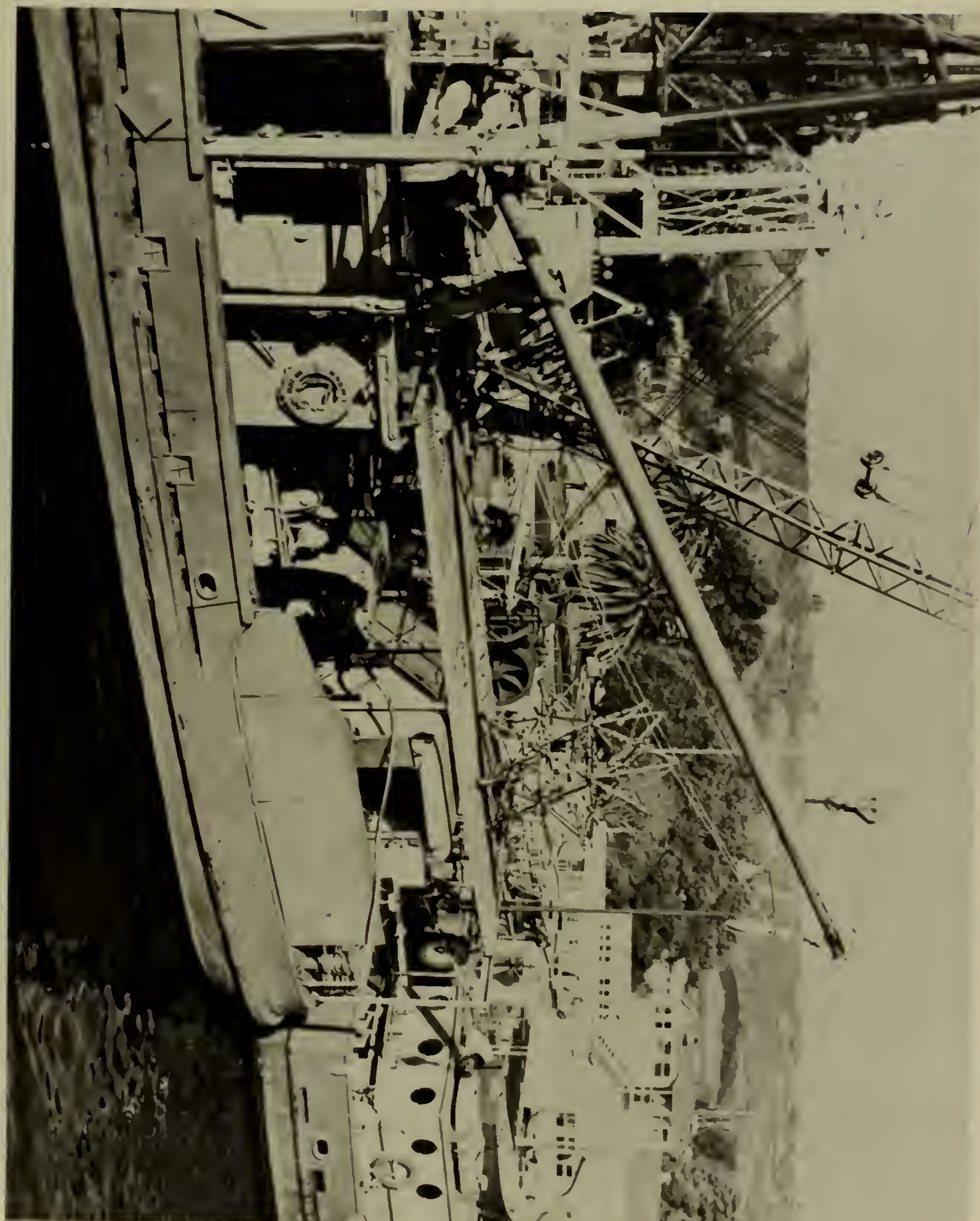

FIGURE 3. AMBIENT NOISE EQUIPMENT

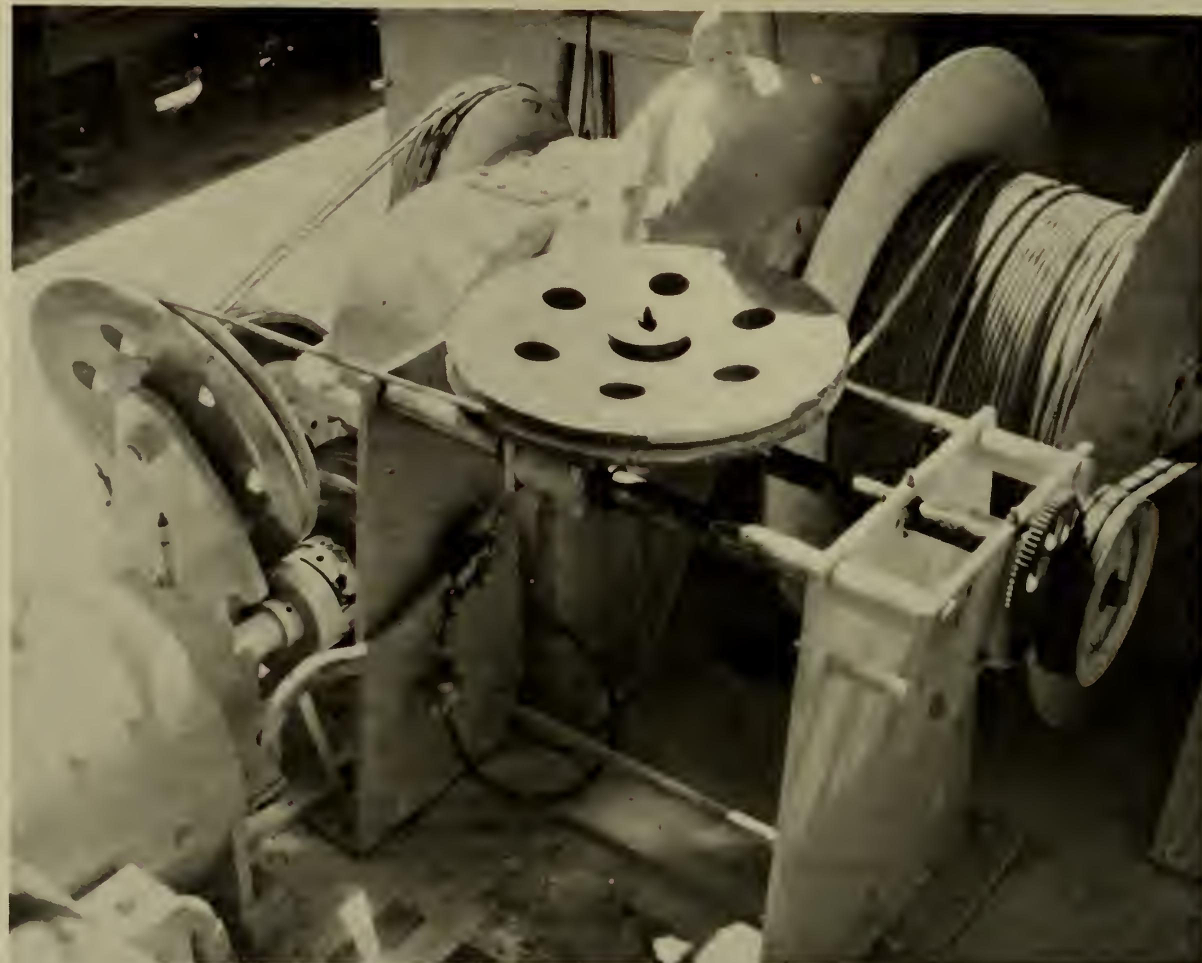

FIGURE 4 AMBIENT NOISE ARRAY WINCH

FIGURE 5. HYDROPHONE / TRANSMITTER ASSEMBLY

samples of the signal which have been clipped is included. Referring to Fig. 6a, the time varying analog audio output of an individual hydrophone channel is shown. Some band limiting has occurred in the hydrophone preamplifier bandpass filters. Further high-pass filtering by the simple network of Fig. 6b removes any remaining fluctuation below the frequency of interest resulting in the waveform of Fig. 6c. The waveform of 6c is transformed into one of two states as shown in Fig. 6d by the clipper amplifiers. Figure 7a repeats Fig. 6d. In addition Figs. 7b, c, d and e represent the outputs of four other channels. The example has been so chosen as to illustrate the array gain of a five hydrophone system in detecting a directional signal mixed with omnidirectional noise. An input signal-to-noise ratio at the individual hydrophone of unity has been assumed. The direct addition of the five output voltages produces a randomly fluctuating voltage as shown in Fig. 7f. The absence of a pronounced peak is to be expected since the noise at each hydrophone due to the isotropic background is uncorrelated while correlation between voltages generated by the directional noise will be visible only when the proper electrical delays corresponding to the geometrical delays between hydrophones are introduced by the shift registers. The voltages of Figs. 7a through c are sampled at the shift register inputs at a 5 kilocycle per second rate. This timing satisfies the Nyquist criterion of a minimum sampling rate equal to twice the highest frequency of the spectrum of interest. Figures 7g through 7k repeat Figs. 7a through 7e with the proper delay introduced by the shift registers to correct for hydrophone geometry. The

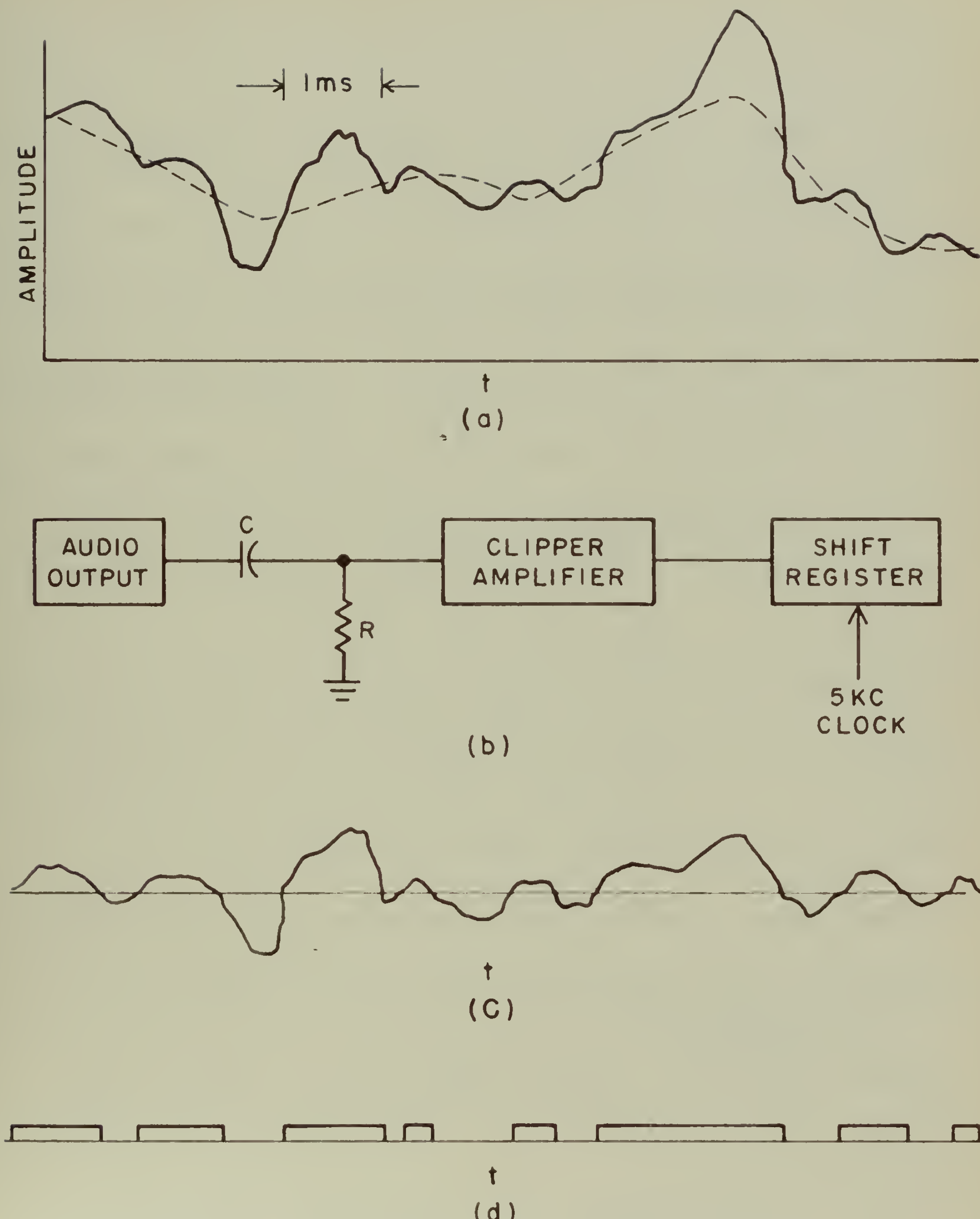

FIGURE 6 CLIPPED PROCESSING

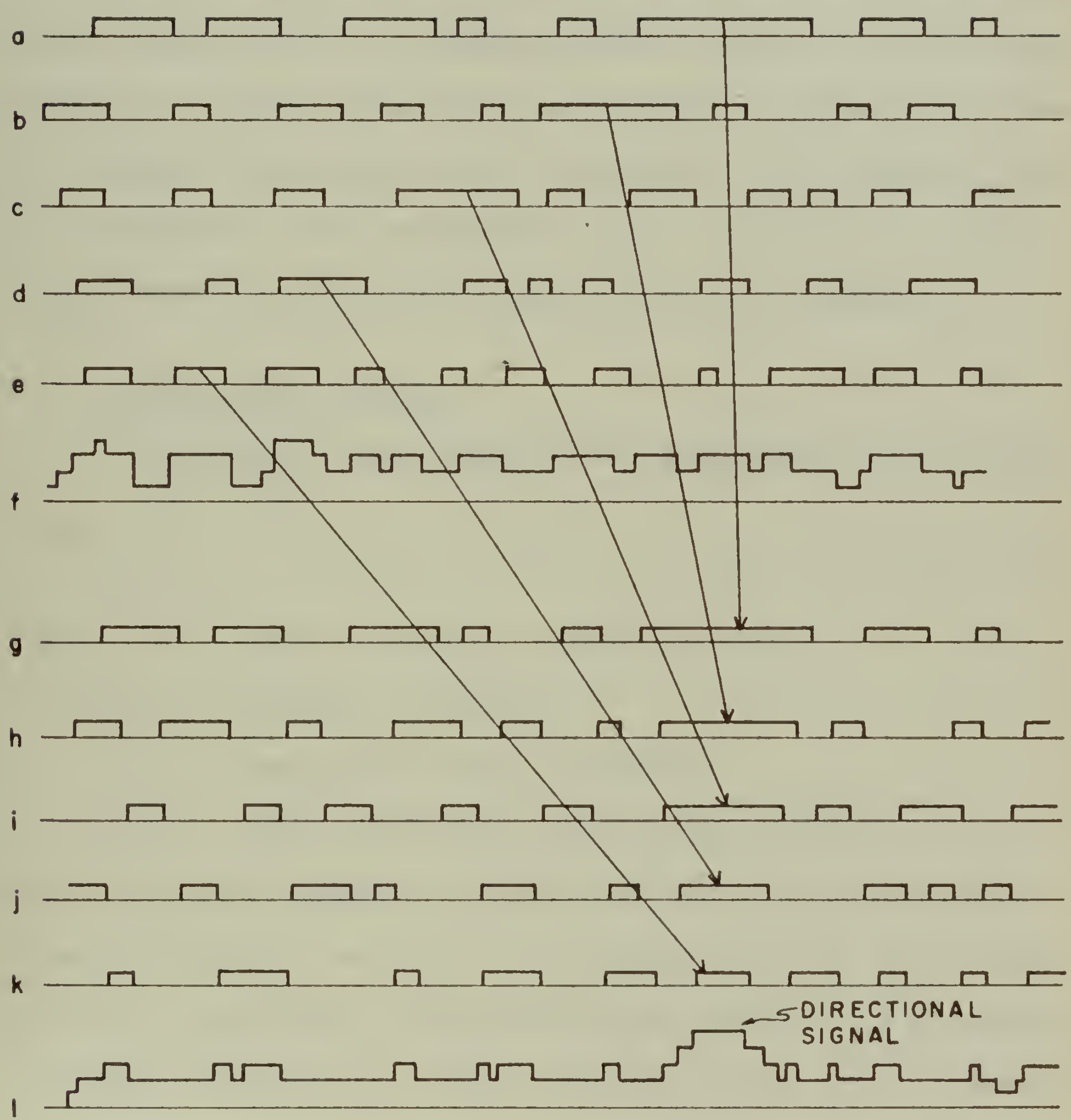

FIGURE 7 THE ADDITION OF CLIPPED SIGNALS

addition of Figs. 7g through 7k shown in Fig. 7l again produces a randomly fluctuating voltage with the exception that now a peak appears due to the directional noise. The reproduction of the original signal improves with the number of channels employed. In aural test with the 32 element system it is not possible to distinguish between an unclipped audio signal input as monitored at the output of a single hydrophone and the reconstituted input as heard at the output of a beam formed from the clipped signals of the 32 elements.

2.6 Array Beam Patterns

The summed voltage output of all hydrophones may be written:

$$e_{out} = \sum_{i=1}^{N} e^{\frac{-j\omega R_i}{c}} \left[\cos(\theta_s - \theta_i)\cos(\phi_s - \phi_i) - \cos(\theta_s - \theta_i + \theta_D)\cos(\phi_s - \phi_i + \phi_D)\right]$$

where ω = angular frequency, radians per second

R_i, θ_i, ϕ_i = hydrophone coordinates

θ_s, ϕ_s = electrically steered direction

θ_D, ϕ_D = angular deviations from steered direction

Due to hydrophone symmetry, a particular beam will exhibit conical symmetry about the beam axis. The icosohedron has two axes of symmetry and, accordingly, two different beam patterns. In a spherical coordinate system with the array center as origin, every element can be pictured as positioned on one of two concentric shells. There are 20 elements located on the outer shell and 12 elements on the inner shell. The two axes of symmetry are formed by lines through the array center and elements on the outer and inner shells. Since each array element has a diametrically located twin, the expression for

power output with $\theta_S = \phi_S = 0$ and $\phi_D = 0$ becomes:

$$G(\theta_D) = \int_{\omega_1}^{\omega_2} \left\{ 2 \sum_{i=j}^{16} \cos\left(\frac{\omega R_i}{c} \cos\phi_i \left[\cos\theta_i - \cos(\theta_D - \theta_i) \right] \right) \right\}^2 B(\omega)\, d\omega$$

where $B(\omega)$ is a weighting function, the relative frequency response of the system and ω_1, ω_2 are the system bandpass limits. Computed patterns normalized to unit on-axis response are shown in Fig. 8. The continuous curve represents the solution to the preceding equation for an outer beam (a beam whose axis passes through an outer element in the array).

The use of the preceding equation as written tacitly assumes that the exact time delay specified by the expression $\frac{\omega R_i}{c} \cos\phi_i \cos\theta_i$ is available. In practice the exact delays are not available owing to the limitations of the digital shift register which at its tapped outputs provides delays equal to integer multiples of the clock generator period. The dashed curve in Fig. 8 is the outer beam response computed on the basis of the actual shift register delays. The dotted curve is the corresponding response for an inner beam. The combined effect of beam differences due to element configurations and steering delays results in an inner to outer on-axis beam response ratio of 0.853, a factor which must be considered in the data reduction process.

2.7 Reduction of External Noise Interference

The preliminary phases of at sea measurements confirmed the existance of two sources of interfering noise which had been anticipated. They were:

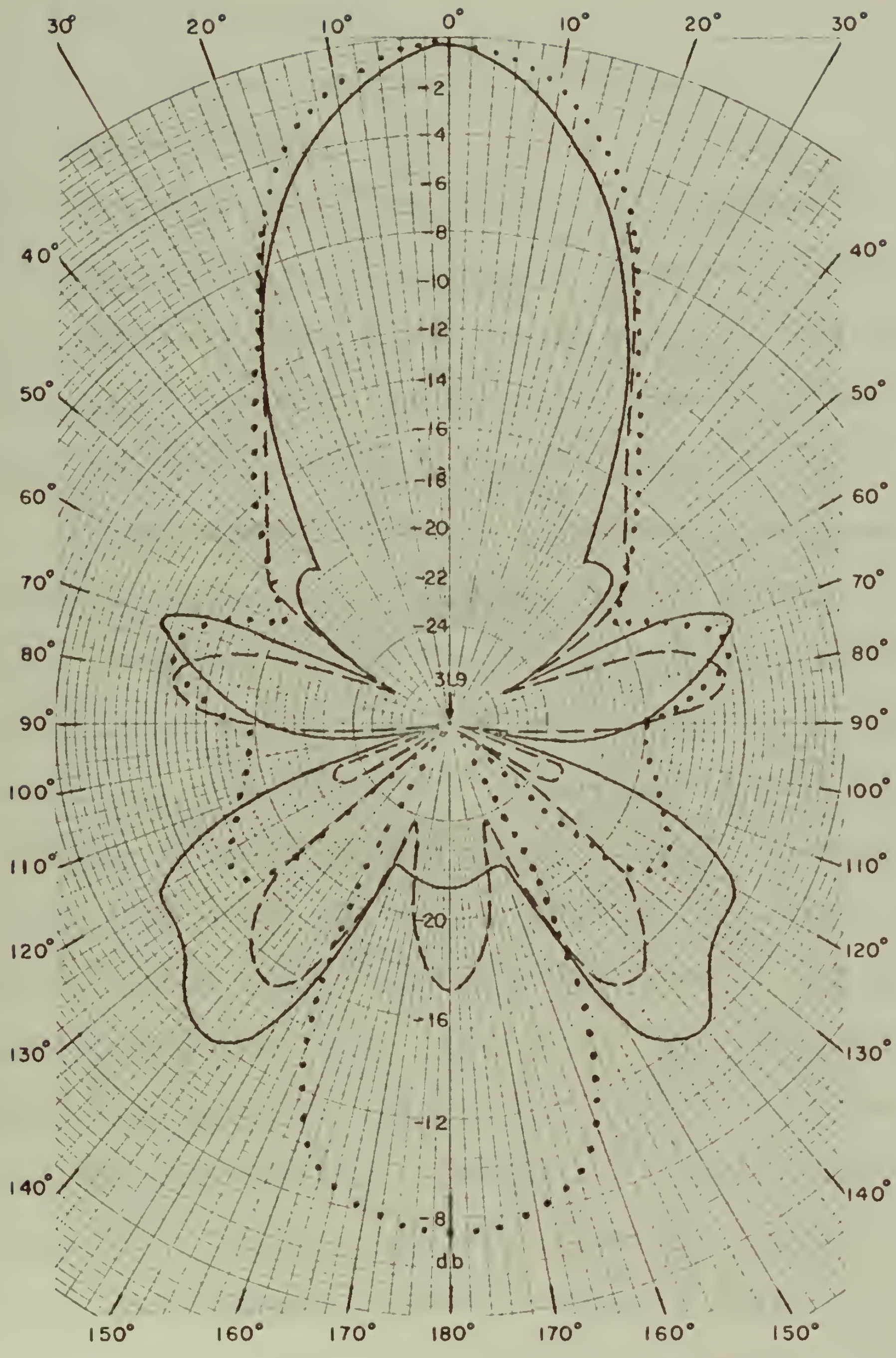

OUTER BEAM (EXACT DELAYS)
OUTER BEAM (SHIFT REG DELAYS)
INNER BEAM (SHIFT REG DELAYS)

FIGURE 8 BEAM PATTERNS

a. Ship machinery noise transmitted through the hull structure into the ocean.

b. Self-noise generated by relative movement of the array and ocean water.

Another troublesome source, external shipping interference, could only be controlled by judicious choice of operating area free from shipping lanes or by testing during night time hours when shipping traffic was at a minimum. A fourth source generated by the rolling motion of the testing ship is discussed in paragraph 5.1.

Own ship machinery noise was eliminated by two means. First, all normal ship machinery was secured during the testing period. Secondly, interference from the special 15 KW gasoline powered generator serving as the power supply for the ambient noise equipment was reduced to a negligible value by isolating the generator from the ship deck by automobile tire casings. The effectiveness of the isolation method was demonstrated by comparative evaluation with a special 5 KW sound isolated unit developed at the U. S. Navy Electronics Laboratory for similar noise tests. This latter source was completely suspended from each of its four corners in a pipe support frame by airplane shock cord. Although its electrical capacity was not adequate for full time employment, alternate operation with first the limited capacity 5 KW unit and then the larger 15 KW source revealed no differences in ambient noise levels as measured at the array suspended in the ocean.

Elimination of the second interfering source, self-noise generated by relative array/water motion, was accomplished by two

means: (1) the suspension of the array from a system of buoys and floats in order to isolate the array from ocean surface and ship motion and (2) the employment of a parachute sea anchor to eliminate ship drift caused by surface winds and attendant array/water relative motion. The two techniques are shown schematically in Fig. 9. The suspension was so designed that the spar buoy would float in the position shown independent of array depth. The floats compensated for cable weight as the array was positioned at 100, 500 or 1000 foot depths. The spar buoy acts effectively as a spring with constant, k, equal to the buoyancy force per length submerged. For the 4 inch diameter buoy in question $k = 5$ lbs/sec^2 which for an array displacement of 500 pounds results in a natural period of oscillation of

$$T = 2\pi\sqrt{\frac{M}{k}} \approx 60 \text{ seconds}$$

a value 10 times greater than the longest period of the ocean waves encountered during the experiment. Particular attention was devoted to buoy swivels and connecting links in order to prevent noise generation by any metal-to-metal contact.

The sea anchor employed was a surplus government parachute fastened in the manner shown by manila hawser and equipped with a manila tripping line for collapsing purposes. Even in very light wind of 7 knots it was effective in maintaining ship's head into the seas, reducing ship roll and completely eliminating drift. Under certain not infrequent conditions stratified ocean currents were experienced where surface currents and wind were in a direction different from the ocean current at the array depth. The net effect was the

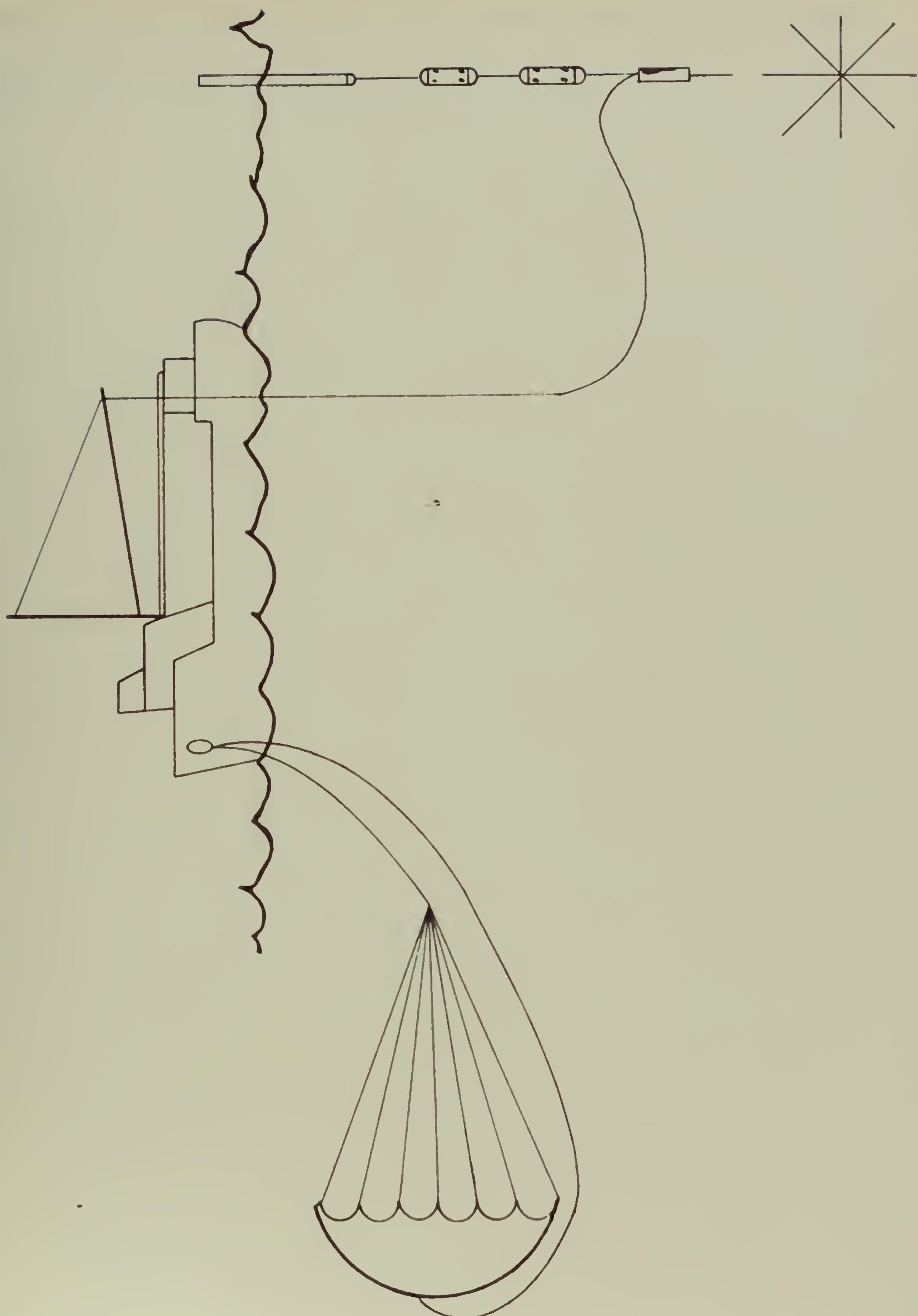

FIGURE 9 SEA TEST CONFIGURATION

towing of the array by the test ship and parachute and invariably resulted in test cancellation.

III. SYSTEM MEASUREMENT ACCURACY

3.1 Discussion

The ideal manner in which to specify system measurement accuracy would be in terms of beam response to a calibrated source capable of producing an output spectrum covering the ambient noise equipment bandwidth. Up to the present the above procedure has not been possible for a variety of reasons. The chief limitation arises from the low frequency of operation of the system. Neither the necessary low frequency broadband source nor a quiet, deep water area with adequate facilities for maintaining array/source geometry has been available for test. Although it has not been possible to calibrate the system as a single unit by one series of measurements, calibration of all component parts of the system, individually, has been possible and is considered an adequate substitution for the single measurement procedure. In paragraphs 3.2 through 3.7 following, the possible error contributions of all component parts of the system are examined. Detector calibration has been established as the major source of error in the system and will accordingly be considered first. It is the objective of the remaining paragraphs to show that all contributions from other components of the system are negligible in contrast to detector calibration error.

3.2 Detector Calibration

The use of clipped processing considerably complicated detector calibration procedures. Since the output amplitude of a given beam is a function of the relative phase correlation between

individual hydrophones and is independent of individual hydrophone output amplitude, the input/output characteristic of a given beam forming/detector combination could not be established by injecting a signal of controlled amplitude into each clipper amplifier and measuring detector output voltage.

The problem is further complicated by the nature of the shift register matrix output. A representative waveform in shown in Fig. 10a illustrating the summed voltage output from 32 shift registers with random noise input. The desired information is contained in the fluctuating AC. The undesired 5 kilocycle per second clock pulses, arising from the particular form of shift register circuitry employed, eliminated the possibility of employing full wave rectification and necessitated use of less efficient half-wave rectifiers. A quantitative analysis of the system output including the effects of clipping is contained in Appendix I.

Although 32 random noise generators whose relative correlations could be varied at will would permit detector calibration, no circuitry to fulfill this requirement was obvious. Instead a perfectly correlated AC signal was employed. A 2.5 kilocycle per second test voltage of two phases, 180 degrees apart, was derived by frequency divider from and synchronized with the 5 kilocycle per second clock generator. Application of one or the other of the two phases to a particular clipper amplifier input would assure that the corresponding shift register outputs were identical, either off or on. By adjusting the number of clipper amplifier inputs of each phase, the matrix output for any beam could be varied from 0 to $\pm$ 16 units.

[illegible]

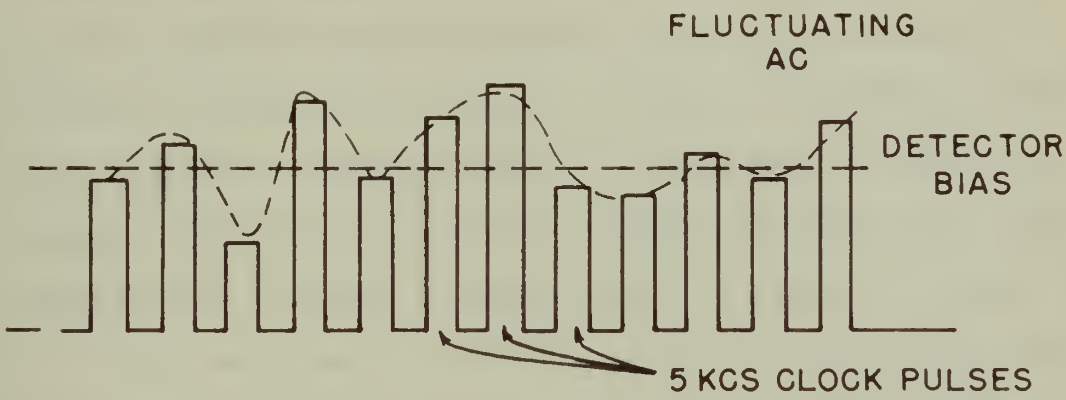

10 (a)

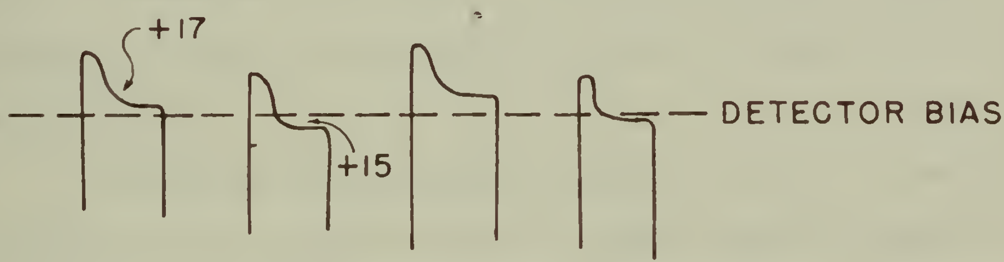

BIAS SETTING PROCEDURE
10 (b)

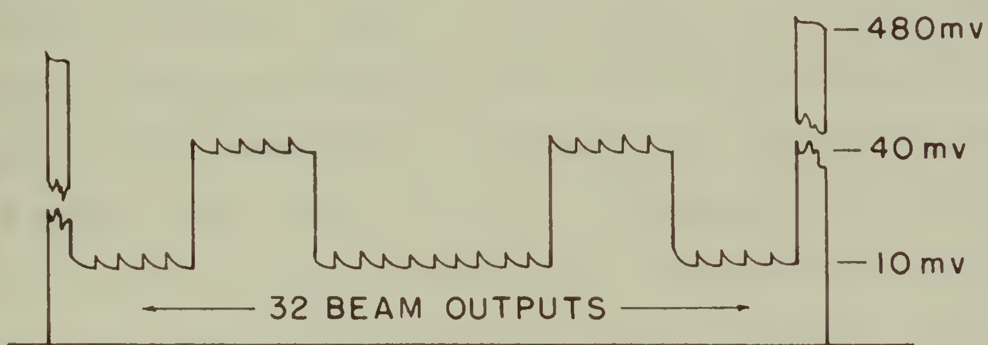

OSCILLOSCOPE TEST PATTERN
10 (c)

FIGURE 10 DETECTOR OUTPUT PATTERN

Detector bias was adjusted so that with 17 inputs of one phase and 15 of the opposite phase, the detector output amplitude was 1/2 the difference in clock pulse amplitudes as viewed by oscilloscope and as shown in Fig. 10b. Transient spikes as indicated in the figure and detector inefficiency prevented the achieving of exactly zero output voltage for the condition of inputs divided equally as to phase.

Time variations in individual detector characteristics were compensated for by trimming each detector bias to permit alignment with a predetermined test pattern as shown in Fig. 10c. This was created by steering the test signal to produce maximum response on beams 1 and 32.

By progressively changing the inputs from half of each phase (minimum detector output) to all of one phase (maximum detector output) complete detector characteristics could be traced. Many tracings for each detector were required to average out the slight differences in individual register outputs emphasized by the artificial nature of the single frequency input but averaged automatically in practice by the random nature of the noise. The applicable portion of a typical curve is shown in Fig. 11. After one set of characteristics had been determined as described, a duplicate set was produced. In no case did the second set differ by more than 1 millivolt from the first set. This 1 millivolt error is considered the maximum system error and amounts to an error in the measurement of the output of any beam of 0.2 decibels.

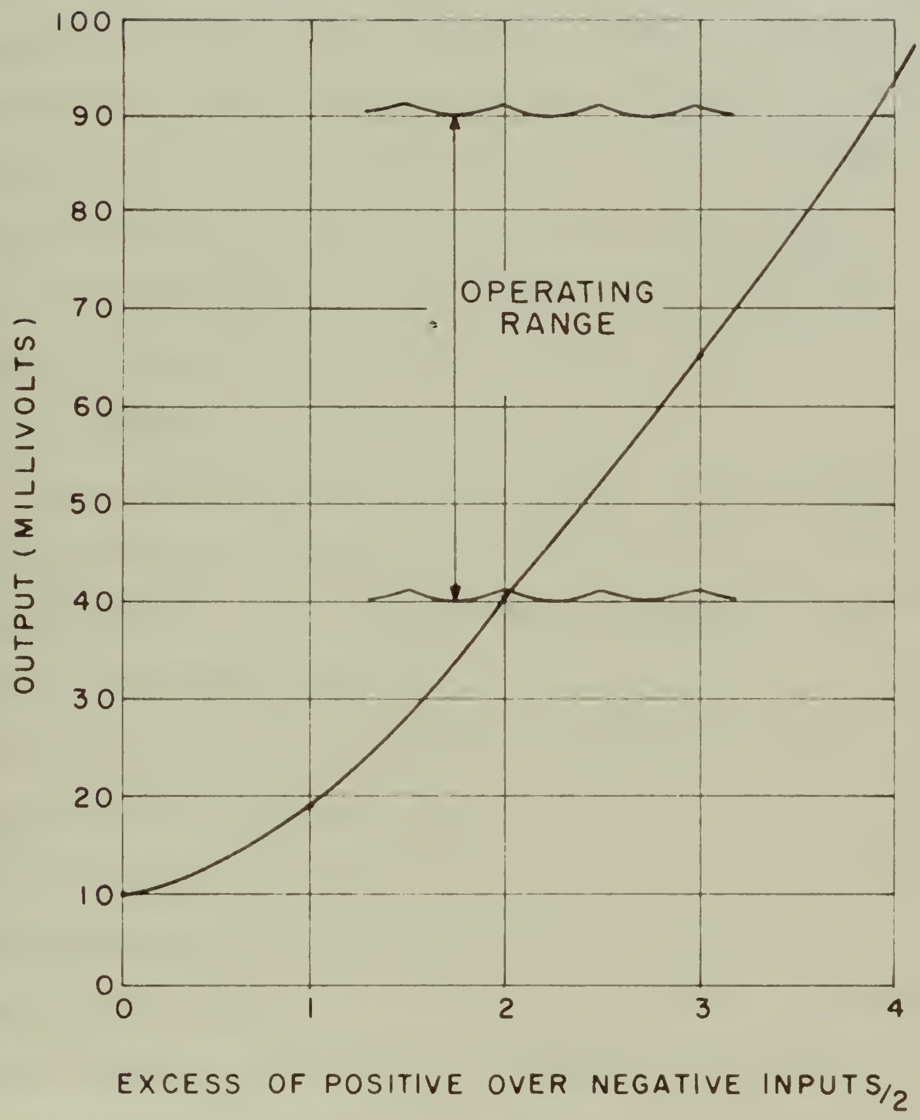

FIGURE 11 TYPICAL DETECTOR CHARACTERISTICS

3.3 The Array

Individual array elements comprising the $BaTiO_3$ receiving unit and the FM transmitter canister housing were calibrated by the U. S. Navy Electronics Laboratory calibration facility at Sweetwater Lake, San Diego, California. Measured horizontal and vertical receiving patterns were completely circular. Since the wavelength at the nominal array center frequency of 1 kilocycle per second is 5 feet, the patterns are understandably uniform indicating that the individual hydrophones are equivalent to a point hydrophone. The cylindrical shape of the hydrophone and canister does not alter the isotropic response.

Although the response of the assembled array of individual elements could not be measured, acoustic theory and World War II measurements(12) of sonar dome structures demonstrated that support members of cross-section equal to or less than 1/15 of a wavelength have no effect upon the beam patterns of arrays transmitting through such structures. Since the ambient noise array support members are 1 inch steel angle iron approximately 1/8 inch thick, the above design criterion is more than adequately satisfied. It is concluded, therefore, that the array may be considered formed of 32 exactly identical omnidirectional receiving elements unaffected acoustically by any supporting structure. Accordingly, it is considered that no errors are introduced by the array.

3.4 The RF System

The RF system was examined as to circuit noise, dynamic range and the introduction of undesired phase shifts.

With an appropriate capacitor substituted for the hydrophone crystal, electronic circuit noise levels averaged 20 decibels below sea state zero noise levels.

The question of dynamic range primarily concerned channel cross-modulation. Modulation levels were adjusted such that maximum noise levels as measured at sea produced no more than a $\pm$ 50 kilocycle per second deviation of the appropriate channel carrier. This adjustment permitted a 100 kilocycle per second separation between channels and eliminated all possibility of cross-talk between channels.

Signal phase shifts unintentionally introduced by receiving channel components are equivalent to electrical time delays. Only differences between channel phase shifts are significant since equal phase shifts in each channel are equivalent to the application of a fixed time delay to all channels which would not affect beam output. Channel phase shift differences will not seriously affect beam output until they approximately equal the sample period of 0.2 milliseconds or 72 degrees. A large relative phase shift would cause the signal to appear at the incorrect shift register tap and would distort the beam pattern. To measure the actual shift introduced by the system from hydrophone to shift register input, conventional Lissajous figure oscilloscope techniques were employed. An audio oscillator output was coupled by suitable attenuators to the oscilloscope horizontal deflection plates. A parallel oscillator output was capacitatively coupled to the hydrophones in air by a special cup designed to fit concentrically over the array hydrophone

elements. The clipper amplifier output of the particular hydrophone channel undergoing measurement was fed to the vertical deflection plates of the oscilloscope. The oscillator frequency was adjusted for a straight line or zero phase shift. For the 32 channels the frequency of zero phase shift was found to vary between ± 30 cycles per second centered at 1.01 kilocycles per second. A second measurement of the phase shift characteristic of an individual channel determined by observing the frequency corresponding to the easily read Lissajous points of 180, 90 and zero degrees permitted conversion of the initial zero phase shift frequency measurement to phase shift at zero frequency. From this latter auxiliary measurement it was established that 0.33 degrees shift occurred per cycle or that the greatest measured shift was ± 10 degrees from 1.01 kilocycles per second, a value well within the sampling period.

It is concluded, therefore, that no significant errors were introduced by the RF system.

3.5 Beam Forming System

Errors in beam output introduced by the beam forming system may occur due to four possible causes:

a. Inadequate clipper amplifier dynamic range.

b. Nonuniformity of clipper amplifier input band-limiting filters.

c. Amplitude variation of shift register outputs.

d. Nonuniformity of matrix summing resistors.

Clipper amplifier dynamic range, defined as that range where clipped output is independent of input amplitude, was measured to be 70 decibels, a value well in excess of the range of ambient noise levels in the ocean. No error is attributed to this source. Anderson[13] has shown that errors in output of individual elements comprising an array degrade the array signal-to-noise output ratio in accordance with the relation:

$$S/N = n(1 - \sigma^2)$$

where n is the number of array elements and σ is the standard deviation of the individual element errors. The standard deviation for items (b), (c) and (d) above when measured individually and then combined was less than 10 per cent. Substitution of this value into the above expression yields a 0.05 decibels loss, a negligible contribution to overall system error from beam forming components.

3.6 Film Recording

As noted in paragraph 2.3, individual beam outputs were photographically recorded continuously throughout each run by 16mm camera. Frame spacing was geared down to 3.5 frames per second. The developed film was viewed for reading on a Craig 16mm Projecto Editor. The displayed frame size was as shown in Fig. 12 where a 40 millivolt calibration pedestal, the base line and 32 beam outputs are indicated. An accurate, fine line, overlay grid of 4 millivolts per division was drawn to large scale and then photographically reduced to the size of Fig. 12. The reading procedure first involved adjusting the projected frame size such that the calibration pulse

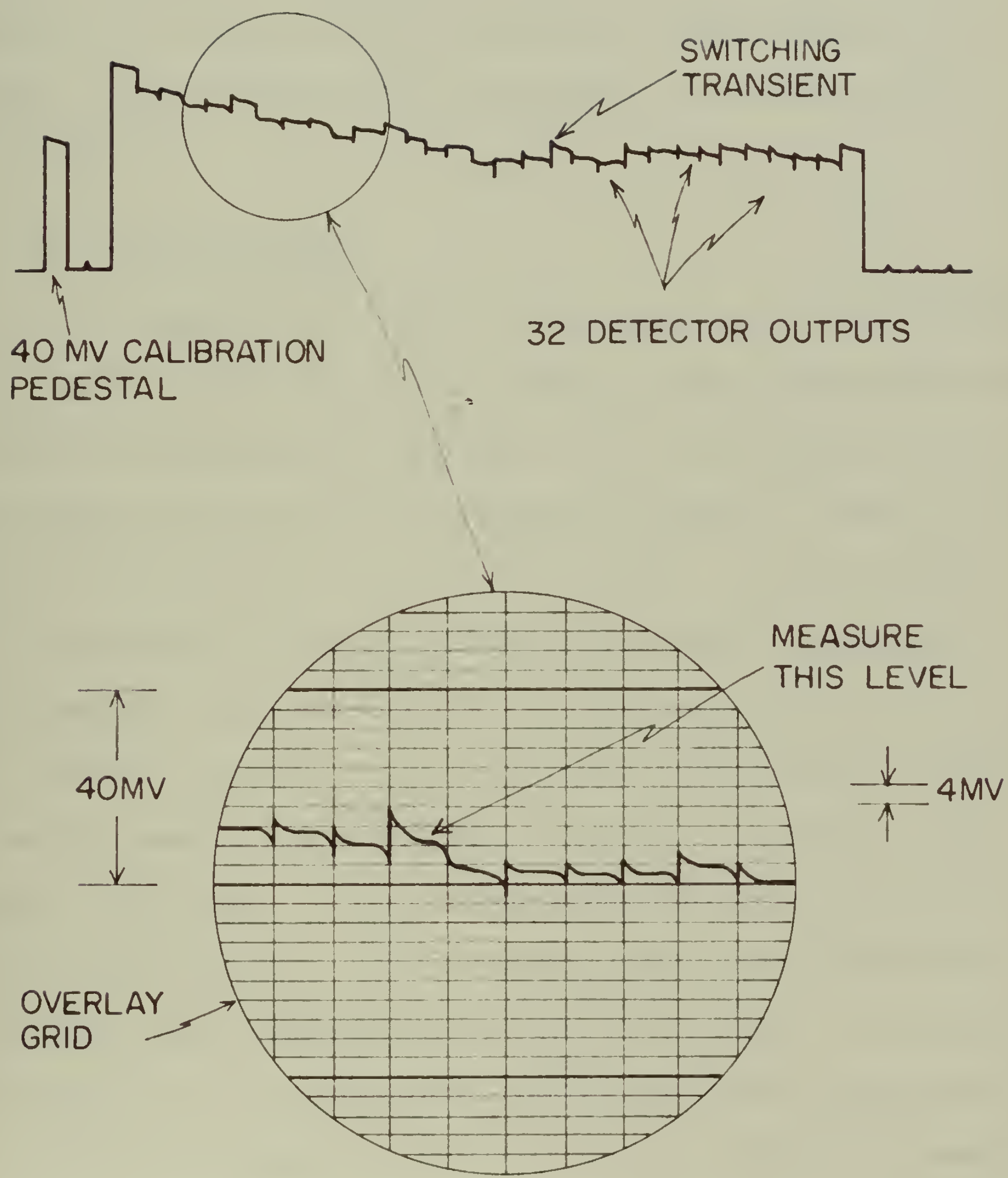

FIGURE 12. FILM RECORD AND OVERLAY MEASURING GRID

height corresponded exactly to 40 millivolts on the viewing grid. The value of each beam output could then be read quite simply to the closest millivolt. Assuming that individual component errors add randomly, the error introduced in the film reading process is considered small in comparison to the detector calibration error of paragraph 3.2.

3.7 System Linearity

A consequence of digital array phasing by the DIMUS technique and symmetry in the array beams is that the sum of the output powers of the 32 array beams is a constant. Thus, an increase in level in a given beam will result in a corresponding decrease in level in the remaining beam outputs. A very strong signal, or its equivalent, good correlation in a given direction, can result in beam capture with resultant suppression of the remaining beam outputs and attendant loss of information as to the relative field intensities viewed by several beams. It is necessary, therefore, to determine that maximum output level on a given beam which does not introduce distortion in the outputs of the remaining beams. Toward that end it is assumed that a signal-to-noise ratio at the input of an individual hydrophone of 1 to 10 represents a sufficiently small signal such as to preclude the possibility of signal capture. The output power generated by such a signal-to-noise ratio has been derived in Appendix II and the results compared to maximum outputs observed during measurements at sea. Since no measured beam outputs exceeded those computed, it is concluded that the system behaved in a linear manner

throughout the experiment.

IV. TEST PROCEDURE

4.1 Narrative

The on-station test procedures were straightforward barring the occasional equipment component failure. Two hours prior to commencement of test the equipment was energized in order to permit a stable temperature to be reached. The detector circuits, for example, proved to be extremely sensitive to temperature changes greater than 1 degree and required thermocouple control of the two electronic equipment hut cooling fans. Upon reaching the test area the parachute sea anchor was rigged and the ship permitted to reach an equilibrium condition headed into the seas. The array was then swung clear of the ship and lowered to within approximately 80 feet of the desired operating depth. The spar buoy and float system was then clamped to the array cable and the system lowered until the weight of the array was supported by the floats. The array was positioned generally between 100 and 150 feet from the ship.

Radar bearings and ranges to any contacts, anemometer readings and fathometer soundings were recorded prior to turning off all ship power with the exception of the ambient noise equipment generator. The detectors were balanced to the calibration signal as described in paragraph 3.2 and an approximate 4 minute film recording made of background noise. Array compass heading, ship's head, swell direction, bearing to the array, oscilloscope and calibration pedestal and base line settings were recorded.

Normally 3 recordings over an hour interval were made at each depth. At the conclusion of a given sequence of recordings at

one depth, ship's power equipment was energized, the array partially raised to permit detaching the float system and then lowered to the new depth. The procedure as described above was then repeated. Approximately 6 hours were required to complete measurements at one station of 3 array depths.

4.2 Test Environment

Tests at sea were planned with the objective of maintaining a constant environment. Since ocean surface effects as noted in Section I were a likely source of non-uniform ambient noise distributions, an effort was made to control other possible variables such as the effects of land masses, surf, shallow water and varying types of ocean bottom. Although it would have been desirable with the above objective in view to conduct all tests in the truly deep ocean beyond the continental shelf, only one such operation was undertaken owing to the limitations in ship speed which dictated a 24 hour one-way travel time to such areas. Only one such extended cruise was undertaken and accounted for all sea state three, 2000 fathom ocean depth data to be reported. The sea state one plus data were obtained in 1000 fathom water in an area which shoaled to 500 fathoms in all directions within approximately 10 miles. The sea state one-half data were obtained in a 1000 fathom area similar to that studied under sea state one plus.

Sea state classifications are at best an approximation even when derived from a stable platform. Since the difficulty of maintaining an objective viewpoint from a rolling and pitching 75 foot

[illegible]

[illegible]

[illegible]

[illegible]

test platform was appreciated, the initially recorded sea state values of two and four were reduced to one plus and three respectively following examination of motion pictures taken at the time of recording. All observations were conducted in moderate swell conditions. The environmental conditions are summarized as follows:

Sea State	Ocean Depth	Array Depth	Type Bottom
3	2000 fathoms	150, 560, 1000 feet	Gray mud
1+	1000 fathoms	150 feet	Gray mud
1/2	1000 fathoms	1000 feet	Gray mud

V. MEASURED DATA ANALYSIS AND RESULTS

5.1 Noise Source Origin

Non-isotropic noise distributions, functions of both azimuth and elevation angle, were measured during the tests described in paragraph 4.2. Observations of the character of the noise fluctuations in the upper beams of the array, namely the vertical upward beam directed normal to the ocean surface and the next family of 5 beams at 38 degrees from the vertical, indicate that one of the several noise generating mechanisms is the white caps of breaking waves. Near the ocean surface individual beam outputs vary considerably from one another in a random manner. Momentary increases in level in a given beam were probably due to the arrival of energy from an individual or small group of white caps or wavelets. As array depth increased, beam-to-beam differences decreased. The logical explanation lies in the increased area of ocean surface subtended by the beams and the liklihood that the beams of a particular elevation angle view more nearly the same distribution of white caps. The above conclusion was substantiated during tests designed to reduce external noise interference described in paragraph 2.6.

Despite efforts to sound isolate the 15 KW power generating equipment during early phases of the experiment, interference from the test ship invariably was observed in that beam most nearly directed at the ship. When installation of special sound isolated generating equipment failed to reduce the interference, further examination revealed that the test ship was unwittingly generating the

equivalent of white caps. The heavy handling boom, rigged to port for all tests created a pronounced list. The list, coupled with a 1 to 2 foot freeboard amidships, resulted in the deck edge dipping below the waves as the ship rolled even in the lowest sea states. A considerable volume of water entered through deck edge scuppers. On the return roll this water would pour from the scuppers on to the ocean surface like water from a pitcher. The process was repeated with each roll. The interference was substantially reduced and the source identified thereby by streamlining the entire portside, rounding over projections and covering scuppers with a 40 foot long, 4 foot wide strip of canvas.

White caps are probably the principal contributor to background noise. However, the ocean surface by some unexplained mechanism still contributes to the noise field at sea states above zero even when white caps are not present. This fact is substantiated by the measured distributions reported in paragraph 6.3.

5.2 Data Analysis

The film data was first reduced to tabular form as described in paragraph 3.6. Three equally spaced 4 minute samples recorded within a 1 hour interval and with an observation every 14 seconds within each sample resulted. The 3 samples for each array position were examined for fluctuations within each sample and between samples. Fluctuations within samples varied from less than $\pm$ 0.4 decibels for beams directed in the lower hemisphere to $\pm$ 1.0 decibels for beams directed upward. The standard deviation of sample

averages was smaller generally than the standard deviation of observations within a sample by the factor $\frac{1}{n}\ y^2$ where n is the number of observations comprising a sample. Accordingly three samples at each depth were averaged and treated as one.

5.3 Azimuthal Dependence

The data were first analyzed for azimuthal dependence by examining the outputs of families of beams of a particular elevation angle. In general, some azimuthal dependence was apparent principally in the outputs of those array beams directed in the upper hemisphere. The distributions normally were elliptical in shape. A representative azimuthal distribution is shown in Fig. 13. It is considered significant that the maximum beam output for a given elevation angle normally aligned itself with the wave fronts of the swells while minimum outputs usually were perpendicular to the swells. This fact suggests a non-uniform radiation pattern of the white cap or wavelet source; transmission in directions normal to the wave front is impeded by the troughs, with lateral transmission along the ridges being less affected.

5.4 Vertical Dependence

The data were examined for non-uniformity in the vertical plane by averaging the outputs of all beams of a given elevation angle, thus eliminating azimuthal dependence. The results are shown in Fig. 14 which presents the measured field as a function of elevation angle for the conditions listed in paragraph 4.2. Sea state

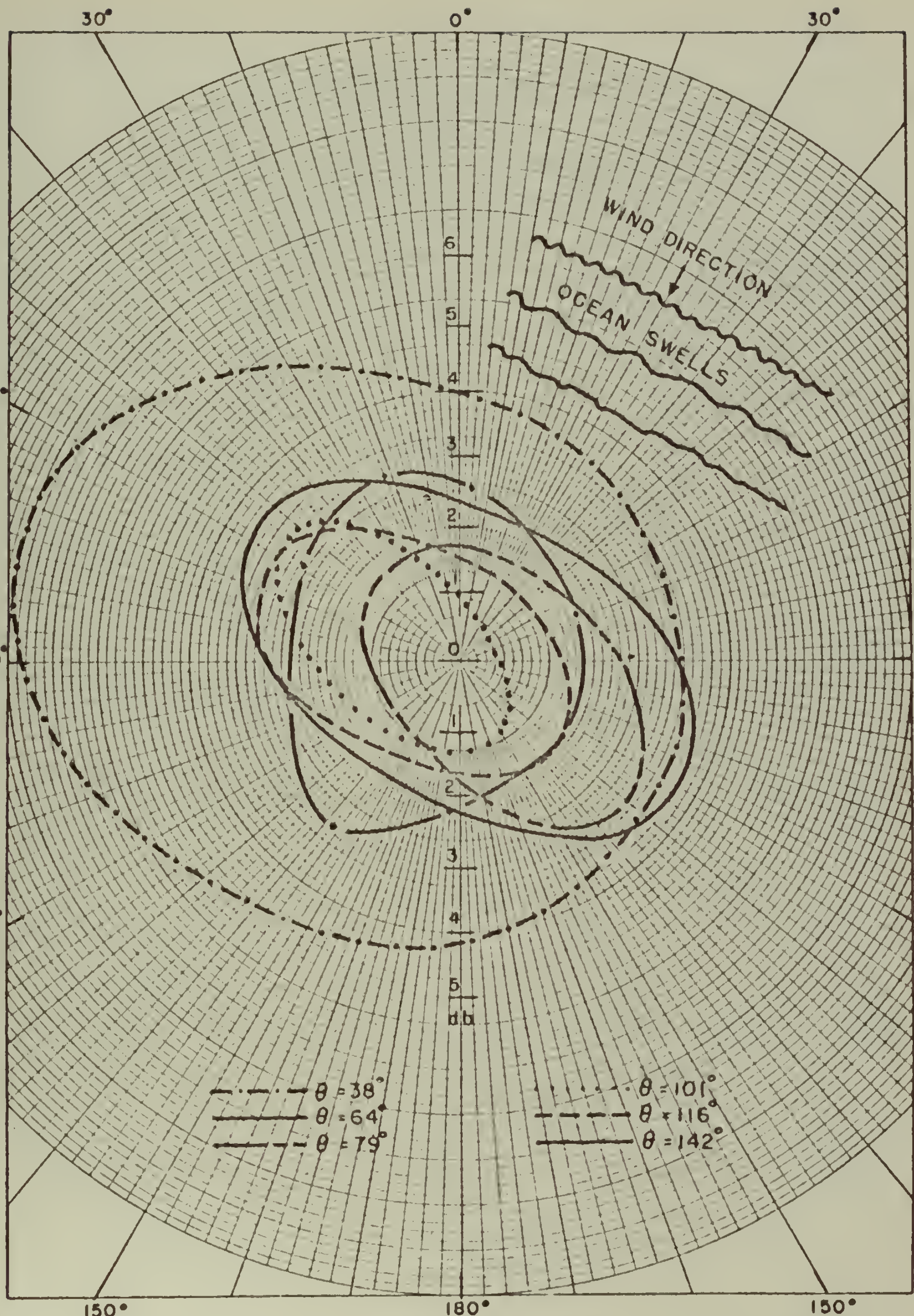

FIGURE 13 AMBIENT NOISE AZIMUTHAL DEPENDENCE
FOR VARIOUS ELEVATION ANGLES (θ)
SEA STATE 3 ARRAY DEPTH 130 FT.

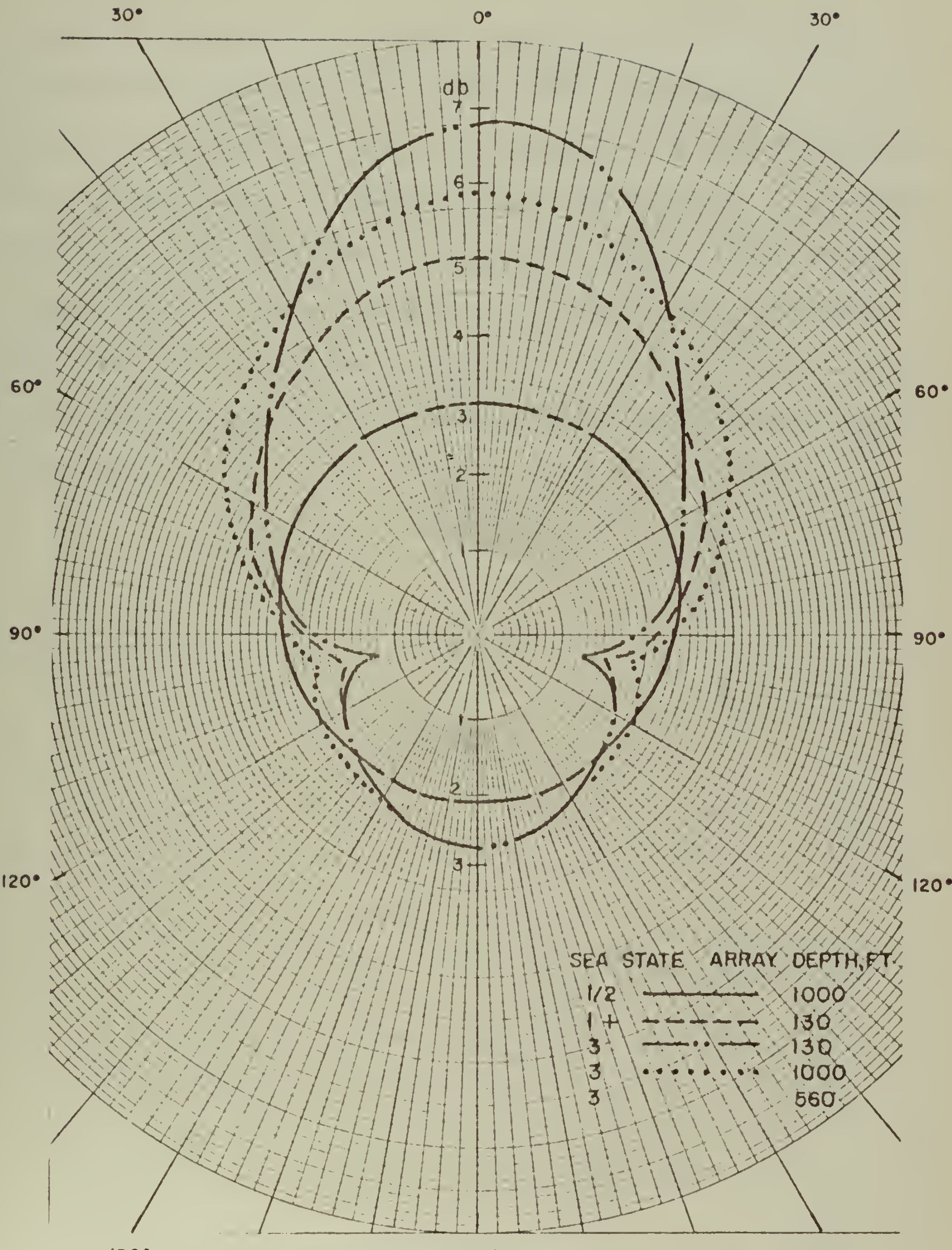

FIGURE 14 VERTICAL DISTRIBUTION OF AMBIENT NOISE VS SEA STATE AND ARRAY DEPTH

effects are apparent with maximum to minimum differences for a given condition varying from less than 1 decibel for sea state one-half to 6 decibels for the highest sea state. Less significance can be attributed to differences in anisotropy magnitude due the variable of array depth because of uncertainty as to the constancy of sea state during the recording period. Approximately 6 hours were required to record data at the three depths during an early morning period of variable winds. It is not unlikely that the recorded sea state of three could in fact have fluctuated between sea state two plus and three plus.

VI. TRUE FIELD RESTORATION

6.1 True Field Indeterminacy

In the preceding paragraphs the analysis has been confined to the measured fields. It is necessary to distinguish between the measured distributions and the true noise distributions. The output from a beam whose axis is oriented in a fixed direction is not determined solely by the true field intensity in the oriented direction. The beam output is proportional to the weighted mean of the intensities in all directions. The weighting factor is the beam pattern. Mathematically expressed, the output of a beam becomes:

$$Y(\theta_B) = \int_{4\pi} G\left[\theta_B - \theta,\ \ \phi_B - \phi\right] X(\theta)\, d\Omega \tag{1}$$

where Y = beam output or measured field.

G = the beam response, a function of the angular difference between axis orientation, θ_B , ϕ_B , and a direction of interest θ, ϕ

X = the true field intensity where, for simplicity, azimuthal symmetry in the noise distribution is assumed.

Since the array beam patterns are not pencil-like with zero response in all but the desired direction but are broad and possess a side-lobe structure as shown in Fig. 8, the effect is to smear the features of the true field.

The problem of reconstructing the true from the measured distribution is common to the field of astronomy where a radio antenna is used to survey the distribution of radio brightness over the sky. The arguments of Bracewell[14] who first considered the problem

in detail in conjunction with aerial smoothing in radio astronomy may be adapted to the underwater acoustics case as follows. Upon integrating over the variable, ϕ , equation (1) becomes

$$Y(\theta_B) = \int_{-\pi/2}^{\pi/2} \bar{G}(\theta_B - \theta) X'(\theta) d\theta \tag{2}$$

where $\bar{G}$ signifies the average of G over all azimuth for a given colatitude and $X' = X(\theta)\sin\theta$. The integral on the right, a convolution integral, may be written

$$Y(s) = G * \underset{\sim}{X} \tag{3}$$

By means of the convolution theorem, equation (3) may be rewritten in terms of the Fourier transforms of the three variables as follows

$$\bar{Y}(s) = \bar{G}(s)\bar{X}(s) \tag{4}$$

where the convolution symbol has been replaced by the algebraic product and the three terms are the spectrums of the corresponding functions of equation (3) and "s" is the number of cycles per unit of angle, θ . From (4) it is seen that $\bar{Y}(s) = 0$ whenever $\bar{G}(s) = 0$ and thus $\bar{X}(s)$ is indeterminate under such conditions. Obviously in any restoration process dependent upon measured values of Y only the low frequency components of X are restored to their full value. The resulting values of X have been called the "principal solution" which may be defined as that solution whose spectrum is the same as the spectrum of the true distribution at all values of s for which $\bar{G}(s) \neq 0$. The results of a restoration process to be described in the paragraphs following, are shown in Fig. 15. The significant feature of Fig. 15 is that the transform of the restored field

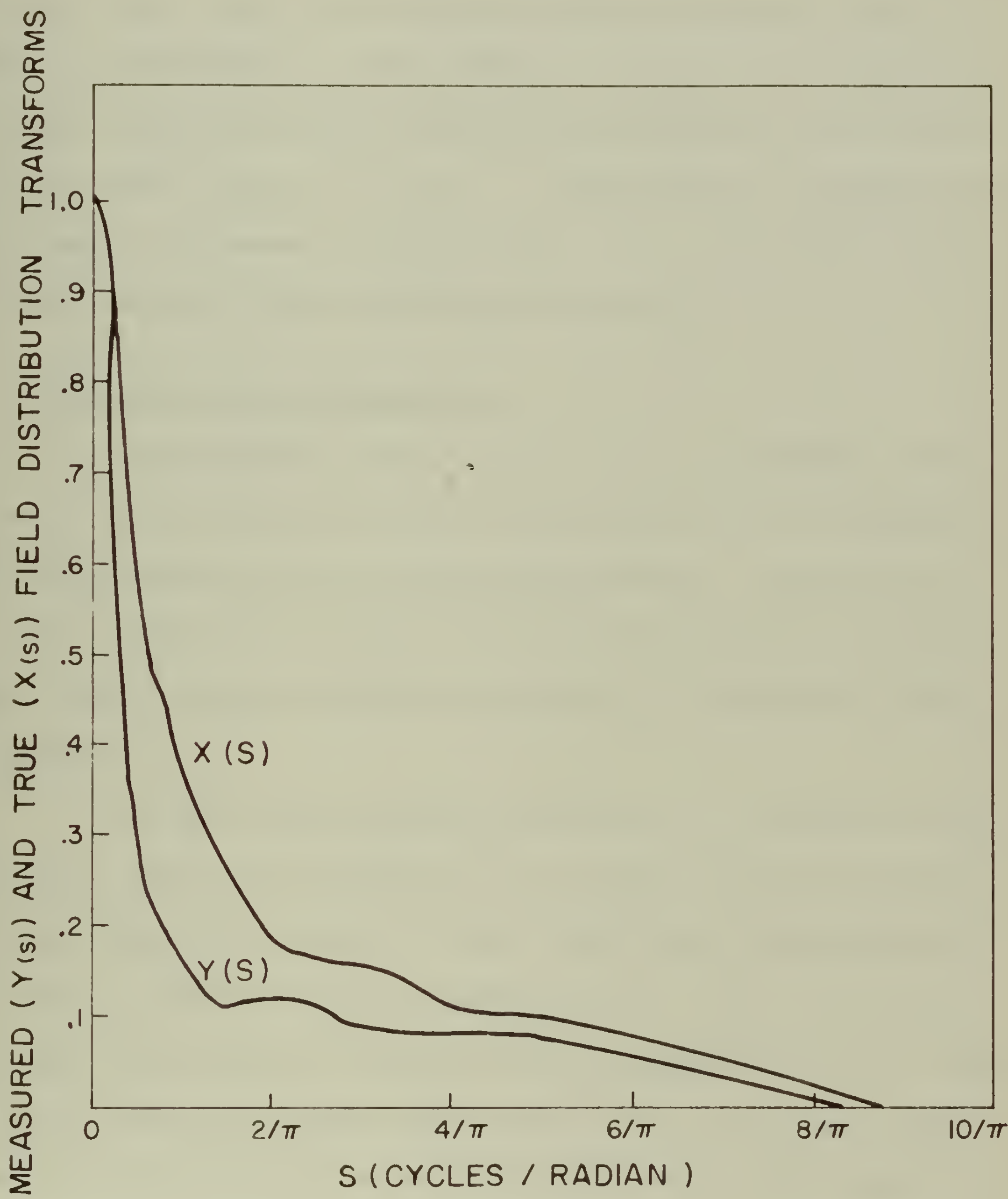

FIGURE 15. DISTRIBUTION TRANSFORMS

approaches zero at almost the same rate as the transform of the measured field. This is an important condition since any values of $\bar{X}(s)$ for s greater than s_k, the value of s where $\bar{G}(s) = 0$, would represent fictitious invisible distributions introduced by the restoration process. Since $X(s_k) \approx 0$, the addition of fictitious high frequency components is negligible and $X(\theta)$ may be considered an exact principle solution throughout this study.

6.2 The Matrix Approximation

The restoration process employed can be considered in two parts: the estimation of a first approximation, and an iterative solution deriving from such first approximation. The former, the matrix approximation, is novel and is considered in this paragraph. The latter, similar to methods of Bracewell, is described in paragraph 6.3.

The matrix approximation is generated by converting the convolution integral of paragraph 6.1 to a finite summation of terms of number equal to the number of beams. Each term in the summation represents a contribution from a particular solid angle and is proportional to the average of the true field subtended by the solid angle. Since a similar expression can be written for each beam, a square matrix results relating values of measured field to the unknown values of the true field. By inverting the matrix, the true field values can be obtained. An exact matrix can be written only for the isotropic case. However, the matrix so derived when used with non-isotropic distributions yields true field values which although

inexact, are closer approximations to the true field distributions than can be arrived at by intuition. The approximation so derived may be then conveniently operated upon by iterative techniques to yield the principal solution. The details of the derivation of the matrix approximation are contained in Appendix III.

6.3 The Iterative Solution

The iterative solution is a method of restoring the true field by successive substitutions. The first approximation previously described is tested by numerically completing the integration of equation (1) of paragraph 6.1, and comparing the results with the measured values of beam power, Y_i . From experience with numerous computations of this nature, it has been determined that a suitable second approximation is obtained by correcting the first approximation by an amount equal to twice the difference in decibels between the measured and computed values of Y_i . Three such iterations were usually sufficient to reduce the difference between measured and computed values to less than experimental measurement error.

Bracewell[14] has shown that a sufficient condition of convergence of the above process it that $\bar{G}(s)$ be non-negative, a condition which is satisfied by the transforms of the beam patterns of the experimental array.

A comparison of the decibel differences between a given pair of beams before and after restoration show a two to three-fold increase in the decibel difference. It is reasoned that measurement

errors will be similarly increased in the restoration process. Accordingly, the errors in the true field principal solution are estimated to be no greater than ± 0.6 decibels except in those regions where abrupt discontinuities in the distributions exist. A sample computation of the complete restoration process is contained in Appendix IV.

The resulting true field distributions for the five environmental conditions described in paragraph 4.2 are shown and tabulated in Figs. 16 through 20. The existance of a marked noise null in the horizontal direction is especially useful in the design of sonar arrays whose objective is to detect weak signals in a noise background. For the detection of horizontally arriving signals in a background of noise arriving from all directions, good vertical directivity as well as horizontal directivity is advisable. To illustrate: consider two arrays of equal horizontal directivity but differing vertical directivity. Let one array have uniform vertical response and the second 20 decibel rejection over all vertical angles except within 15 degrees of the horizontal. The signal-to-noise ratio of the latter array will be 5.5 and 8 decibels better than the former when both are positioned in an isotropic noise field and the field of Fig. 16 respectively.

As previously noted, variations in the noise field distribution for differing array depths could not be established because of uncertainty as to the constancy of sea state during the recording period. The increase in anisotropy with increasing sea state, however, is obvious.

COLATITUDE (θ) DEGREES	LEVEL db $\overline{re}\ \theta = 0°$
0	0
10	− .8
20	− 1.8
30	− 2.7
40	− 3.4
50	− 3.8
60	− 4.1
70	− 5.1
80	− 6.7
90	− 7.7
100	− 8.1
110	− 8.0
120	− 7.6
130	− 6.9
140	− 6.7
150	− 7.2
160	− 7.7
170	− 8.1
180	− 8.2

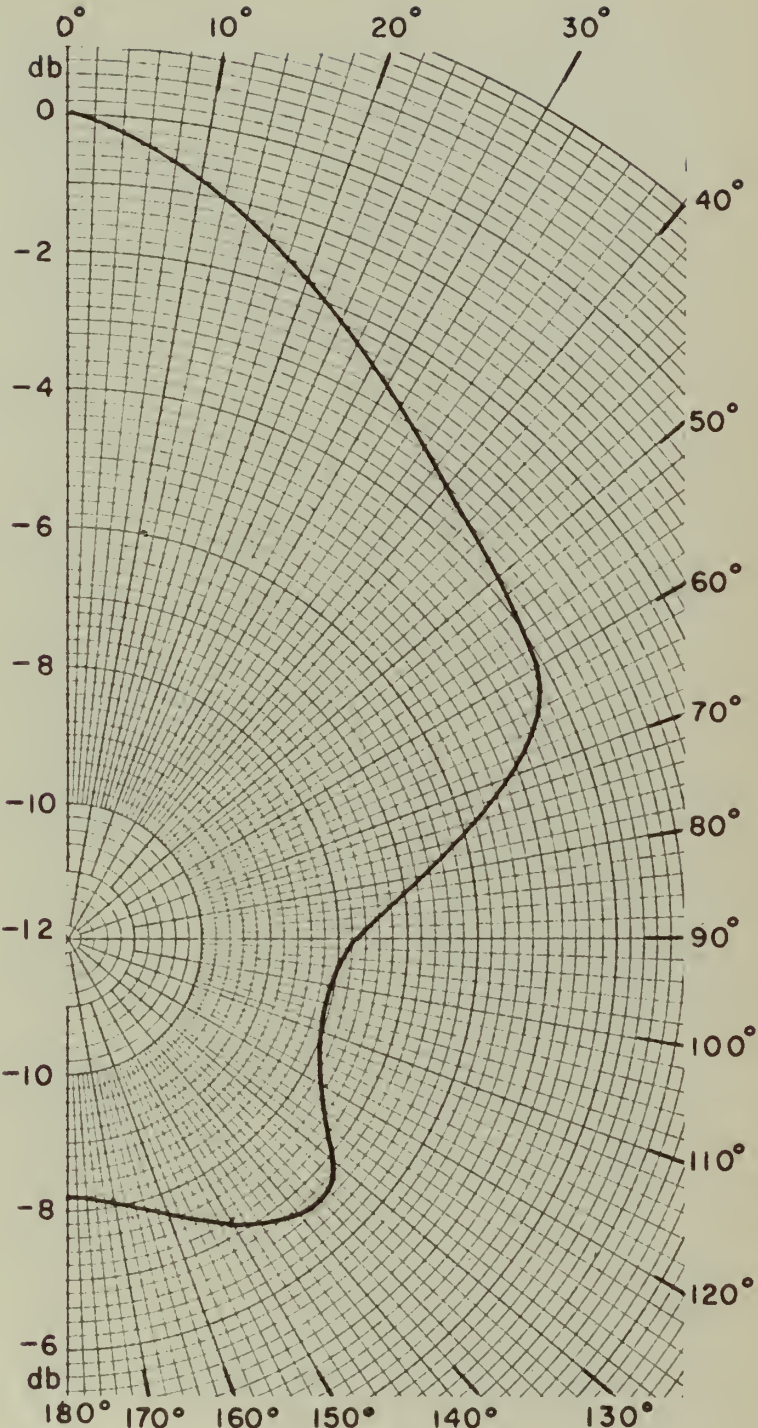

FIGURE 16 TRUE FIELD VERTICAL DISTRIBUTION
SEA STATE 3 ARRAY DEPTH 1000'

COLATITUDE (θ)	LEVEL db re $\theta = 0°$
0	0
10°	− .6
20°	− 1.9
30°	− 3.4
40°	− 4.8
50°	− 5.9
60°	− 6.6
70°	− 7.3
80°	− 7.5
90°	− 10.0
100°	− 11.5
110°	− 9.7
120°	− 8.5
130°	− 8.5
140°	− 9.0
150°	− 9.6
160°	− 10.1
170°	− 10.5
180°	− 10.7

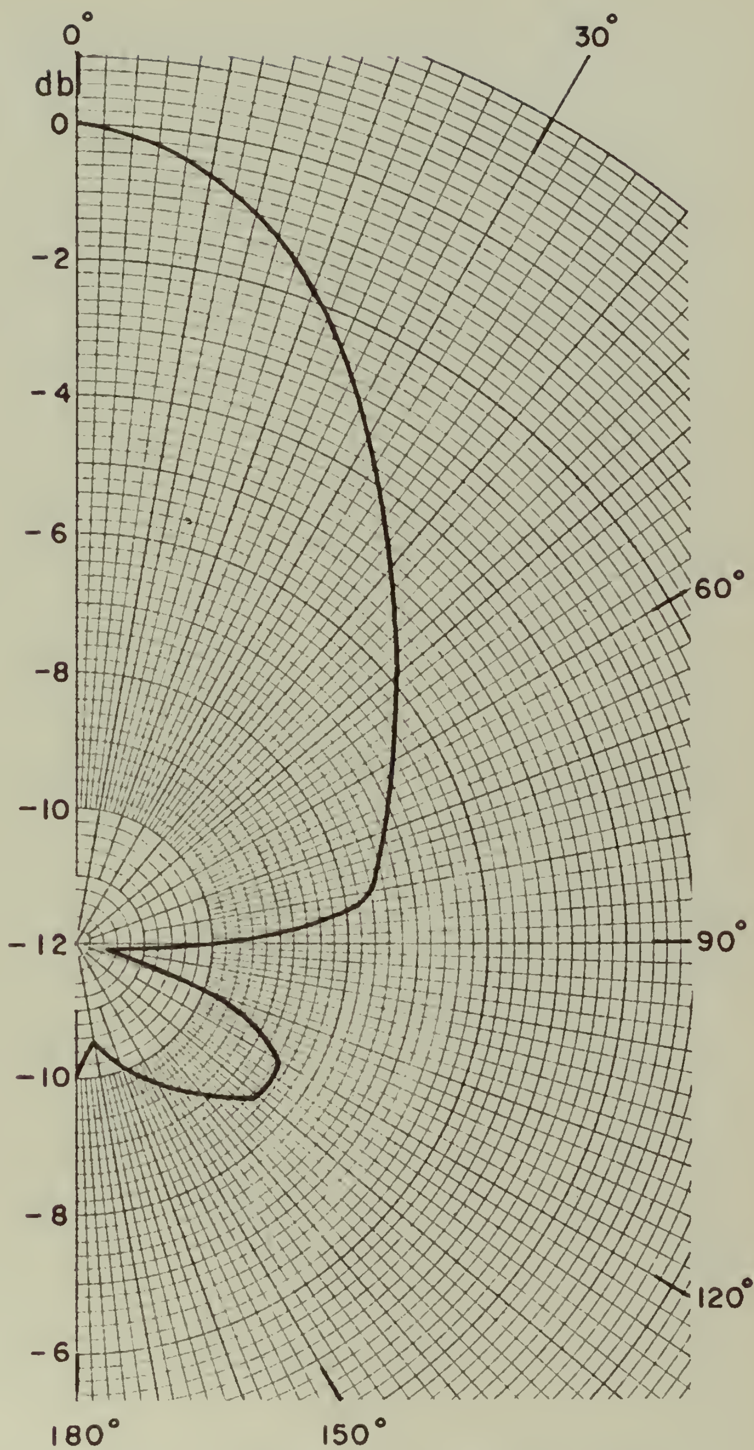

FIGURE 17 TRUE FIELD VERTICAL DISTRIBUTION
SEA STATE 3 ARRAY DEPTH 560 FT

COLATITUDE (θ)	LEVEL (db) re θ = 0°
0°	0
10°	-1.5
20°	-3.3
30°	-4.7
40°	-5.6
50°	-6.3
60°	-6.9
70°	-7.6
80°	-8.5
90°	-10.0
100°	-10.8
110°	-10.2
120°	-9.6
130°	-8.6
140°	-7.8
150°	-8.5
160°	-9.3
170°	-9.8
180°	-10.0

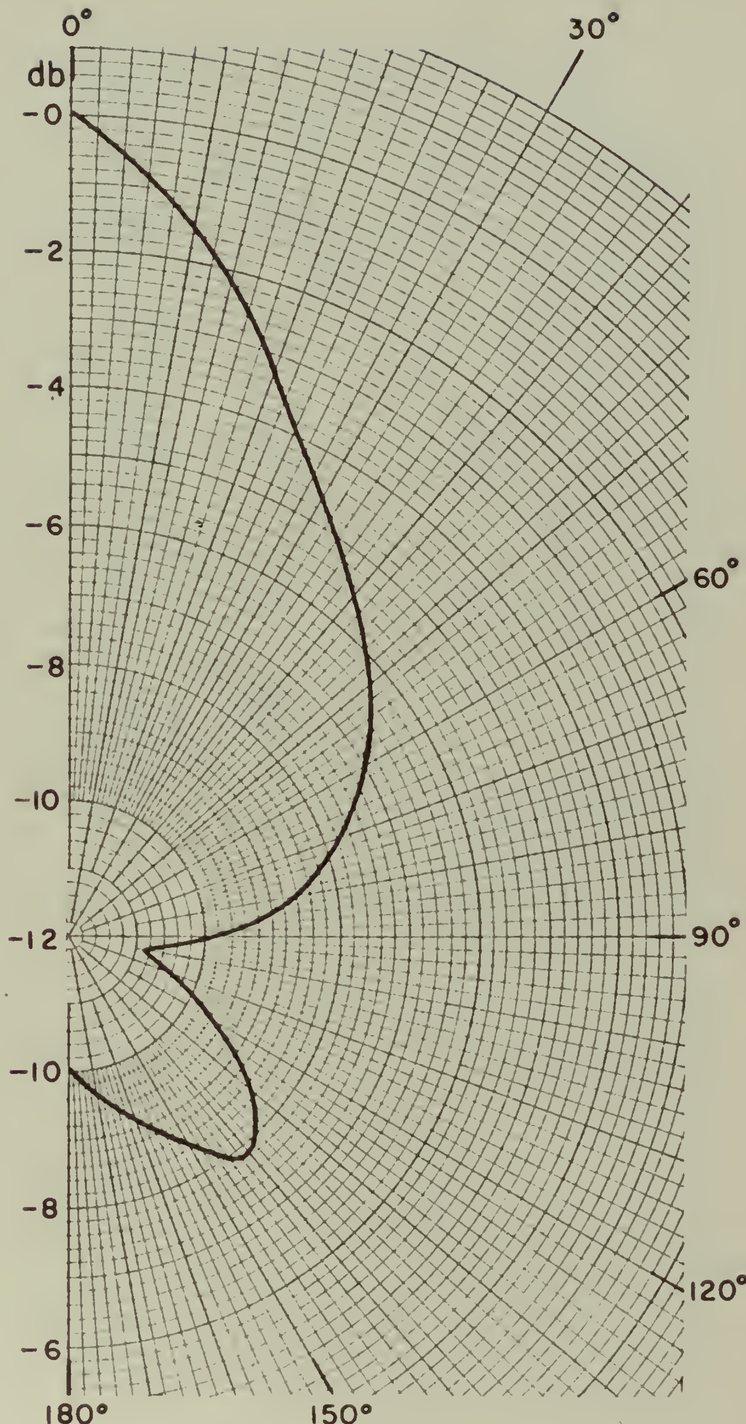

FIGURE 18 TRUE FIELD VERTICAL DISTRIBUTION
SEA STATE 3 ARRAY DEPTH 150 FT.

COLATITUDE (θ)	LEVEL (db) re θ = 0°
0°	0
10°	− 1.1
20°	− 2.1
30°	− 2.9
40°	− 3.3
50°	− 3.6
60°	− 3.7
70°	3.8
80°	− 5.3
90°	− 6.5
100°	− 7.6
110°	− 7.0
120°	− 5.8
130°	− 5.1
140°	− 4.8
150°	− 4.7
160°	− 4.8
170°	− 5.2
180°	− 5.7

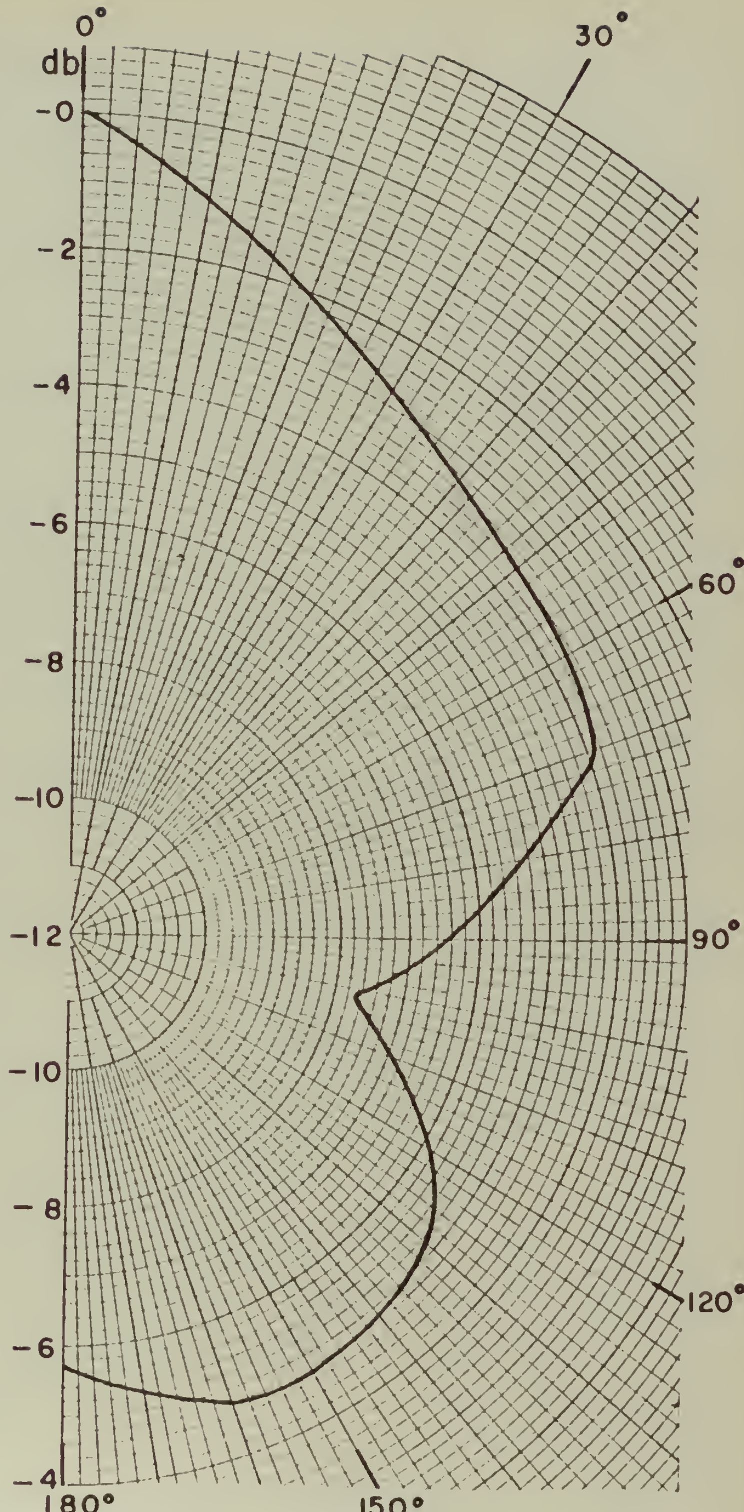

FIGURE 19 TRUE FIELD VERTICAL DISTRIBUTION
SEA STATE 1^+ ARRAY DEPTH 130 FT.

COLATITUDE (θ) DEGREES	LEVEL db re θ = 0°
0	− 0
10	− .2
20	− .37
30	− .5
40	− .6
50	− .65
60	− .67
70	− .78
80	− 1.06
90	− 1.73
100	− 2.25
110	− 1.43
120	− 1.00
130	− 1.10
140	− 1.23
150	− 1.34
160	− 1.40
170	− 1.40
180	− 1.40

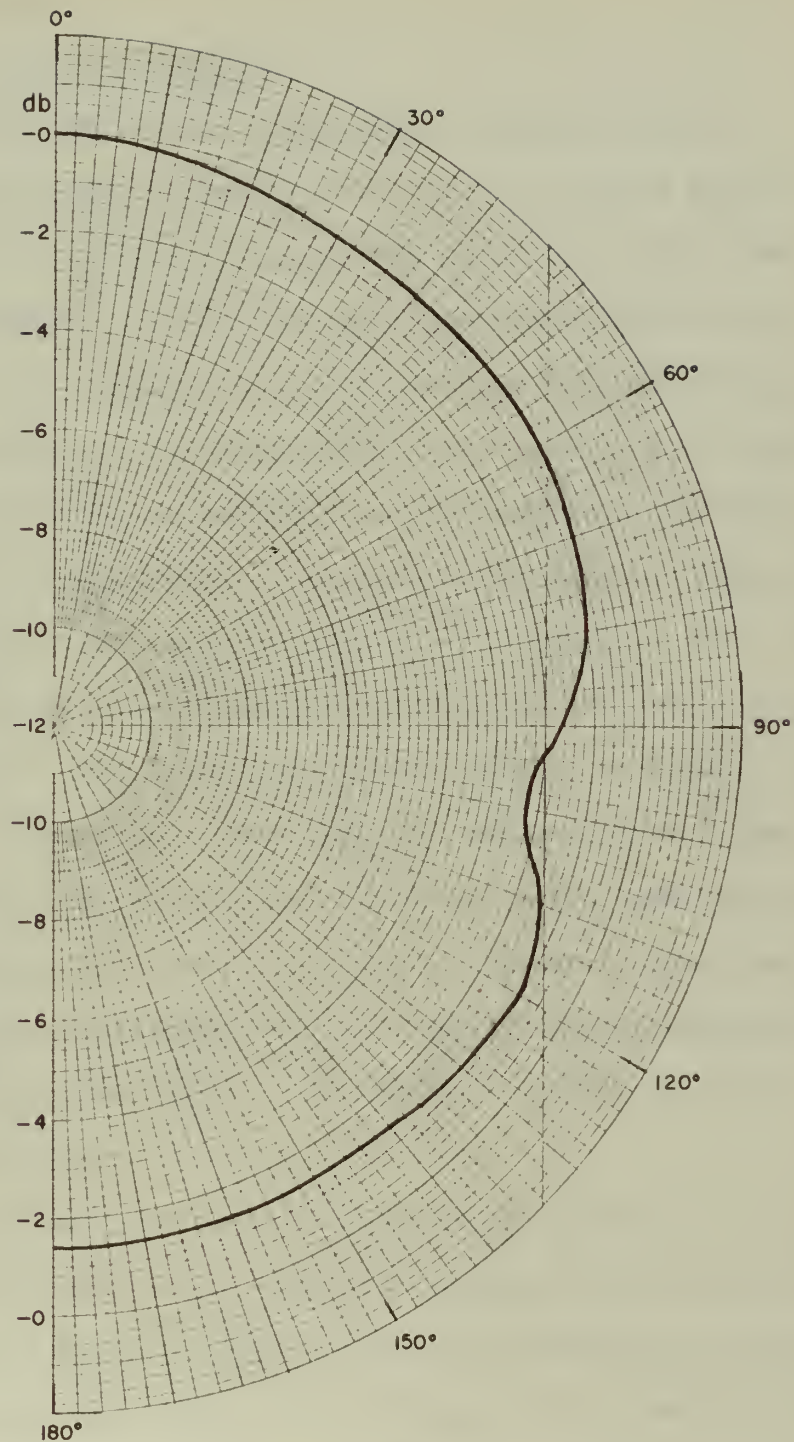

FIGURE 20 TRUE FIELD VERTICAL DISTRIBUTION
SEA STATE 1/2 ARRAY DEPTH 1000FT

VII. AN OCEAN MODEL

7.1 Ocean Model Development

From the nature of the distributions shown in Figs. 16 through 20 and consistent therewith, the following simple picture of the mechanism of noise generation and redistribution in the ocean has been constructed. Noise in the deep ocean is presumed to be a superposition of two fields. The first field is that which exists at sea state zero prior to the development of wave motion and/or white caps. Its distribution is isotropic and its origin was not established during this experiment. A possible explanation of the origin of low sea state ambient noise is considered in paragraph 8.1. The second source of noise is generated by wave motion and white caps at the ocean surface. The equivalent surface radiator is highly directional in the vertical plane when azimuthal effects are averaged. The directionality can possibly be attributed to the ocean waves and swells functioning in a manner analogous to angular focusing reflectors. In addition, in azimuth the ocean swells impede transmission at shallow transmission angles in directions normal to the wave fronts of the swells.

It is further postulated that the noise intensity at a given point in the ocean due to the equivalent surface radiator arrives by both a direct ray path and single bounce path experiencing specular reflection at the ocean bottom. The intensity at the surface source experiences inverse square spreading loss and absorptive attenuation of the form $10^{\frac{-aR}{10}}$ where "a" is the absorption coefficient (decibels/kiloyard) and R is ray path length in kiloyards.

Referring to the model of Fig. 21 and disregarding for the moment the low sea state isotropic contribution to the total noise field, the above postulation of an ocean model may be restated in mathematical form as follows:

$$X(\theta)\, d\Omega = \frac{S(\theta)\, dA}{R_D^2}\, 10^{\frac{-aR_D}{10}} \tag{1}$$

where $X(\theta)\, d\Omega$ = noise intensity per incremental solid angle at the receiver in the upper hemisphere

$S(\theta)\, dA$ = noise intensity at one yard per incremental radiating surface.

Since

$$d\Omega = \frac{dA \cos\theta}{R_D^2} \tag{2}$$

equation (1) may be rewritten as

$$X(\theta) d\Omega = \frac{S(\theta)}{\cos\theta}\, d\Omega\, 10^{\frac{-aR_D}{10}} \tag{3}$$

or, finally,

$$S(\theta) = X(\theta) \cos\theta\, 10^{\frac{aH\sec\theta}{10}} \qquad 0 \leq \theta \leq \pi/2 \tag{4}$$

A similar expression for the intensity at the receiver in the lower hemisphere due to bottom reflection may be written

$$X(\theta_R)\, d\Omega = \frac{S(\theta)\, dA\, \alpha(\theta)}{(R_{R1} + R_{R2})^2}\, 10^{\frac{-a(R_{R1} + R_{R2})}{10}} \tag{5}$$

where $\alpha\ (\theta)$ is the intensity bottom reflection coefficient and is the supplement of θ_R.

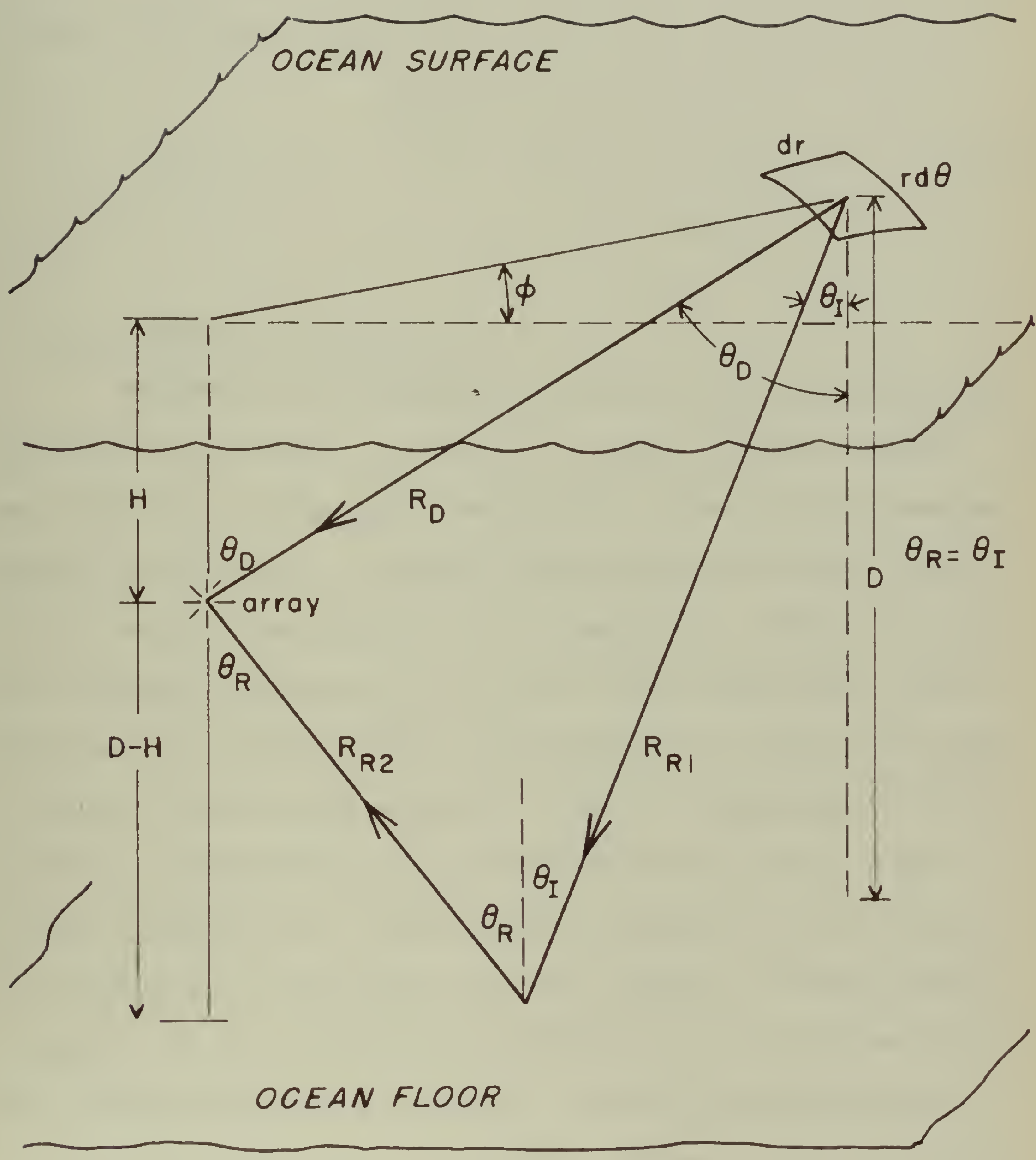

FIGURE 21 OCEAN MODEL

Since

$$d\Omega = \frac{dA\cos\theta}{(R_{R1} + R_{R2})^2} \tag{6}$$

equation (5) may be written as

$$\alpha(\theta) = \frac{X(\theta)}{S(\theta)} \cos\theta \, 10^{\frac{\alpha(2D-H)}{10}\sec\theta} \qquad \begin{array}{l} 0 \le \theta \le \pi/2 \\ \pi/2 \le \theta_R \le \pi \end{array} \tag{7}$$

7.2 Deduced $S(\theta)$ and $\alpha(\theta)$

Employing the distributions of Figs. 16 through 19 and equations (4) and (7) above, values of $S(\theta)$ and $\alpha(\theta)$ were computed. It was necessary to estimate the contribution of the isotropic zero sea state noise field and to subtract that amount from the total field, $X(\theta)$, prior to proceeding with the computation. Several alternative methods of estimating the zero sea state contribution, none of which can be considered exact, are possible. For example, the level of the null occurring at an elevation angle of approximately 100 degrees in all distributions may be considered due to the low sea state isotropic field. Errors in this assumption are likely due to the difficulty in establishing the true minimum. The most probable point of error in the restored distribution is at the minimum due to the difficulty inherent in resolving a sharp discontinuity with a broad beam pattern array. In addition, contrary to the very simple straight ray assumptions of the ocean model, curved path arrivals direct from the surface or by convergent zone paths[6] due to vertical velocity gradients probably contribute to the null level. For

example, Bell[15] has considered the deep ocean case with negative gradient to deep depth. He reports bottom reflection losses for grazing angles of incidence which are approximately 6 decibels less due to the refractive effect of the negative gradient than would be predicted on the basis of straight ray path assumptions.

The best estimate of the isotropic contribution utilized the Knudsen[2] sea state/noise level curves. If the restored distribution is averaged over $4\pi\Omega$, the relative level derived from an omnidirectional hydrophone can be obtained. Subtracting from this level the decibel difference between the Knudsen noise level for the sea state under consideration and sea state zero, the level of the isotropic contribution can be established. The weakness in the above approach rests in its dependence on subjective estimates of sea state level. The error introduced by this technique decreases with increasing sea state since the percentage contribution to the total field of zero sea state isotropic noise becomes smaller under such conditions.

Figure 22 is a plot of $S(\theta)$, the surface source radiating pattern, deduced by the above procedures from the restored fields of Figs. 16 through 20. A reasonable approximation to $S(\theta)$ is the function:

$$S(\theta) = (\cos\theta)^{\frac{90-\theta}{10}} \qquad 0 \leq \theta \leq 70°$$

$$S(\theta) = \cos^2\theta \qquad 70° \leq \theta \leq 90°$$

which is shown superimposed on the experimental data.

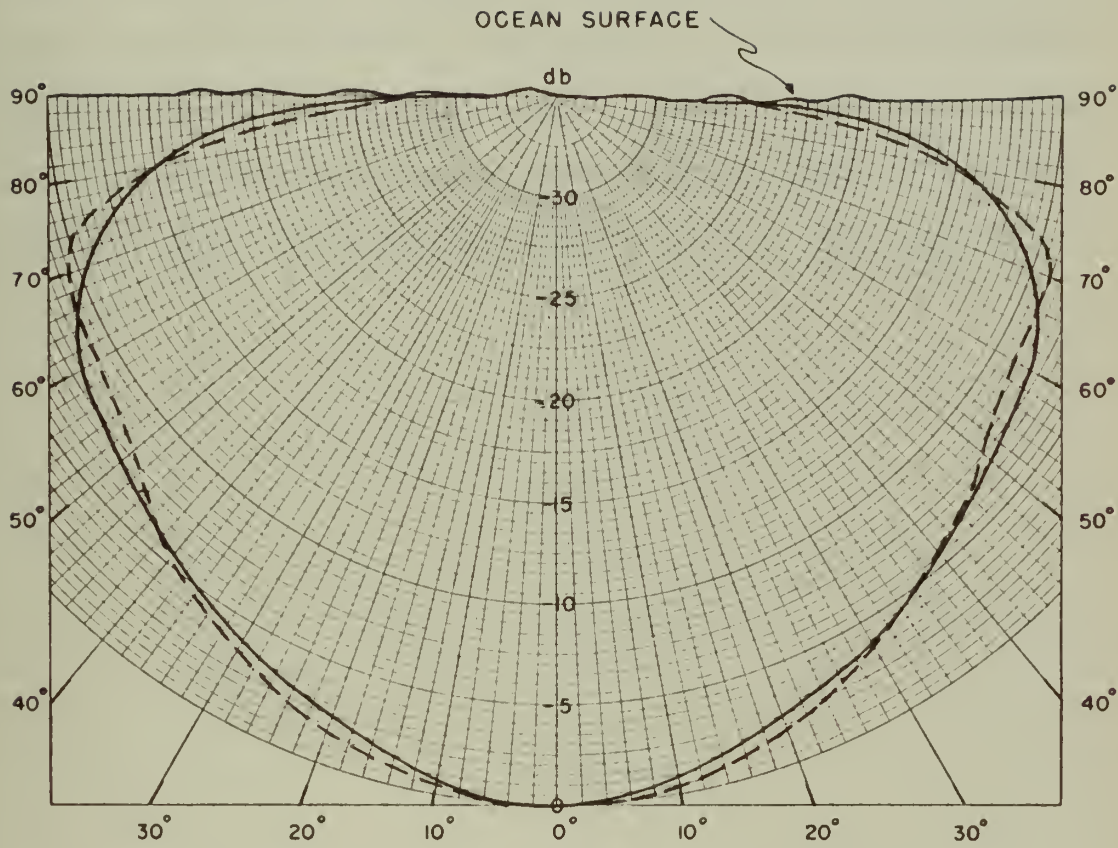

SURFACE SOURCE LEVEL re NORMAL TO OCEAN SURFACE

MEASURED DATA

———— $10 \log (\cos\theta)^{\frac{90-\theta}{10}}$ $0 \le \theta \le 70°$

– – – – $20 \log (\cos\theta)$ $70° \le \theta \le 90°$

FIGURE 22 SURFACE SOURCE RADIATION PATTERN

The bottom reflection coefficient (reflected pressure/incident pressure) derived for conditions corresponding to Fig. 22 are plotted in Fig. 23 together with experimental data and theoretical plots from MacKenzie[16] and Marsh[17]. The fit is considered good in view of the indirect manner in which the data were obtained and the several assumptions involved in the analysis. The results are considered to substantiate the simple ocean model proposed.

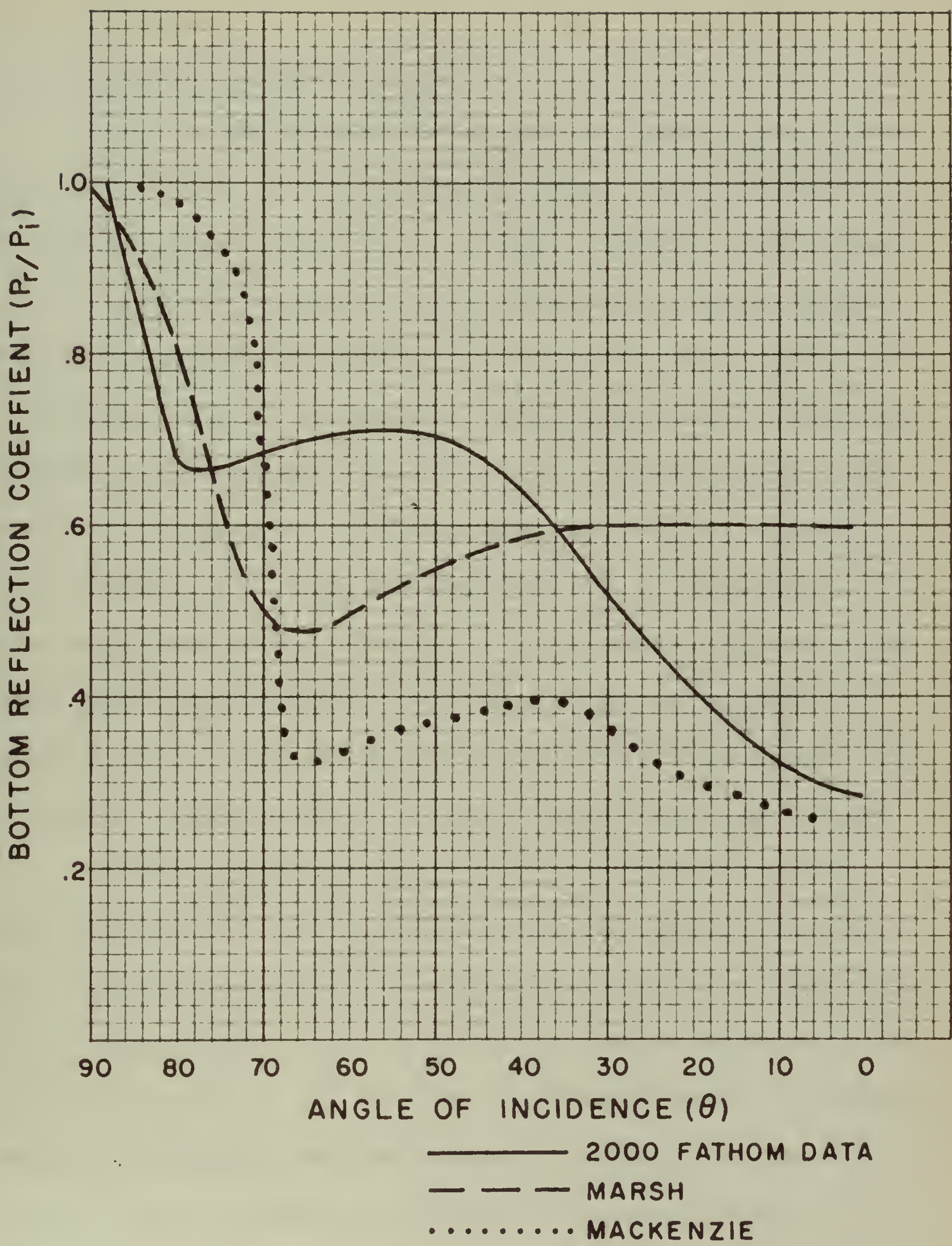

FIGURE 23 BOTTOM REFLECTION COEFFICIENTS

VIII. SUMMARY

8.1 Conclusions and Discussion

Prior to this experiment, as noted in Chapter I, no experimental data existed to describe the directional distribution of deep ocean ambient noise. Accordingly, stated objectives of this study were to investigate anisotropy of ocean ambient noise, to isolate vertical and azimuthal dependencies, to establish the identity of sources contributing to non-uniform distributions and to infer the radiation patterns of such sources. All the above research objectives have been realized by this experiment. Deep ocean ambient noise is anisotropic in the frequency band 750 to 1500 cycles per second and at sea states above zero. Vertical and azimuthal dependencies have been isolated. The surface of the ocean has been identified as a major contributor to non-uniform distributions and the radiation patterns of such surface sources have been deduced.

Vertical anisotropy arises from the superposition of a noise field due to the radiating ocean surface upon an isotropic field present in the absence of surface radiation. The shape of the vertical distribution, Figs. 16 through 20, may be compared to the form of an arrowhead. The arrow tip is directed normal to the ocean surface and represents maximum intensity arriving from the surface direction. The arrowhead tail indicates noise originating at the ocean surface which has been specularly reflected from the ocean floor. A dip in the arrowhead tail in a direction normal to the ocean bottom is evidence of a lower value of bottom reflection coefficient for normally incident sound than for other angles. A

marked null at the waist of the arrowhead, approximately contained within ± 15 degrees of the horizontal, exists in the vertical distribution. The magnitude of the null varies between 2 and 12 decibels below the maximum intensity normal to the surface for sea states one-half to three respectively. The null is due to two effects. First, contributions from the surface source to the horizontal or near horizontal distribution arrive from greater distances than contributions to the off-horizontal distributions and have experienced, therefore, greater attenuation from spreading and absorption. Second, the level of radiation from the surface source in horizontal directions is more than 20 decibels below the level of radiation in the downward directions.

The non-uniform noise distribution with a minimum in the horizontal direction is of practical importance to the design of sonar receiving arrays. The importance of vertical directivity to the detection of horizontally arriving signals is apparent.

The origin of the isotropic zero sea state noise field was not established by this experiment. Of the various sources considered by Frosch(1) distant surface motion is considered most likely. Although the sea surface may be flat at the point of measurement, the noise produced by distant surface disturbances can propagate very long distances with negligible attenuation due to absorption in the 750 to 1500 cycle per second frequency band observed. The scattering and reflection processes experienced by the sound in reaching the point of observation could destroy its original character and an isotropic field result.

Ocean swells are probably responsible for azimuthal anisotropy by impeding transmission of surface generated noise in directions normal to the wave front of the swells.

The intensity at a receiver due to a unit incremental surface radiator of intensity, $S(\theta)$, at one yard, can be considered as the sum of intensities due to direct transmission and specular bottom reflection with attenuation due to spherical spreading and absorption occurring over the separation between radiator and receiver. The quantity, $S(\theta)$, is markedly directional in the downward direction and can be represented approximately by the expression:

$$S(\theta) = \begin{cases} (\cos\theta)^{\frac{90-\theta}{10}} & 0 \leq \theta \leq 70^\circ \\ \cos^2\theta & 70^\circ \leq \theta \leq 90^\circ \end{cases}$$

The above ocean model is not unique. It does, however, conform to the measured data as evidenced by the reasonable agreement between bottom reflection coefficients determined from this experiment and values reported by other investigators. Further additions to the model, as for example the consideration of bottom/surface multiple reflections, are obvious. Such refinements would presume, however, a knowledge of bottom topography and array position relative to the bottom greater than existed during the experiment.

Although the data upon which the ocean model is based were obtained in ocean depths greater than 1000 fathoms, there is no known feature of the model which would preclude its application to shallower depths of perhaps 100 fathoms. Its application to even

shallower depths will depend upon the presently unknown effect of water depth upon the nature of the surface source radiation pattern.

On the basis of measurements conducted over a one hour period under constant conditions of array orientation and sea state, the ambient noise field can be considered stationary. A single, trainable and tiltable directional receiver could be employed, therefore, to duplicate the performance of the 32 element, multibeam array. However, to achieve beam patterns equivalent to those of the 32 element array with a single directional unit, focusing reflectors of dimensions comparable to the 32 element array would be required. A very difficult problem of mechanical training and elevating the reflecting unit would be substituted for the comparatively simple telemetering problem associated with the 32 element array.

8.2 Suggestions for Further Experiment

The results contained herein represent only a first step in the area of ambient noise directional distribution investigation. Objectives for future experiment should include:

a. Shallow water investigation.

b. Extension to higher sea states.

c. Extension to array depths of at least 5000 feet.

d. Extension of bandwidth covered from less than 400 cycles per second to 5 kilocycles per second.

e. Investigation of the effect of land masses such as islands and the continental shelf and the influence of surf.

An additional area of investigation is to substantiate theoretically and experimentally the radiation pattern deduced from this experiment of a white cap situated on the crest of a swell.

ACKNOWLEDGEMENTS

Numerous members of the staff of the Marine Physical Laboratory, of the Scripps Institution of Oceanography, University of California, La Jolla, contributed to the success of this project including the crew of the Scripps motor vessel, PAOLINA T. Special thanks go to Mr. Earl Squier for his assistance in all engineering phases of the project; to Dr. V. C. Anderson who conceived the project and was ready to advise throughout the project; to Dr. P. Rudnick for his frequent advice and counsel and to Professor Leonard Liebermann for his assistance and guidance in the preparation of this thesis.

APPENDIX I

QUANTITATIVE SYSTEM ANALYSIS

The objective of this section is to derive an expression for the voltage appearing at the output of a given beam detector for a random noise input.

Consider first an N element array of omnidirectional elements situated in an isotropic noise field of purely continuous spectrum. If the hydrophone electrical outputs generated by the noise field are summed, with or without the introduction of an electrical delay, and if the hydrophones are sufficiently widely spaced such that cross-correlations between elements are zero, the array output following square law detection will be proportional to $N^{1/2}$. If the cross-correlations are not equal to zero, the output will be proportional to $N^{1/2}(1+e)^{1/2}$ where

$$e = \frac{1}{N} \sum_{i \neq j}^{N(N-1)} \sum \rho_{ij}(0)$$

and ρ_{ij} is the normalized cross-correlation function derived from the input noise spectrum. The value of "e" may also be determined from the directivity ratio. Utilizing the beam patterns of paragraph 2.6, the directivity ratio is derived by numerical integration from the expression

$$\frac{1}{D.R.} = \frac{4\pi}{\int_{4\pi} G(\theta,\phi)\, d\Omega}$$

where $G(\theta,\phi)$ is the beam pattern of paragraph 2.6, and $G(0,0) = 1$.

The quantity, "e", may be determined from the expression $N/1 + e = 1/D.R.$ For inner and outer beams "e" has been computed to be 0.25 and 0.02 respectively. Lawson[17] has shown that the correlation functions of unclipped and clipped signals are related by $\rho_{ij_{\text{clipped}}} = 2/\pi \arcsin \rho_{ij_{\text{unclipped}}}$. For small values of correlation as is the case under consideration, the arcsine of the argument is equal to the argument and the correlation function of the clipped signal reduces to $2/\pi$ times the unclipped correlation function. Since the actual detector employed was a linear rectifier rather than a square law device, an added factor $K = 0.8$ is required. $K = \sqrt{2/\pi}$ is the ratio of the mean absolute value to the root-mean-square value in a normal distribution. A further factor of 0.5 is introduced because the scale of the abscissa of Fig. 11 is 16 for maximum detector output rather than 32. The detector output voltage is therefore proportional to

$$\left(\frac{N}{2\pi}\right)^{1/2} \left(1 + \frac{2}{\pi} e\right)^{1/2}$$

Substitution of the values $N = 32$ and $e = 0.25$ into the above expressions produces the value 2.44. This quantity when entered as the abscissa of Fig. 11 indicates an output value of 52 millivolts for detector No. 1, an inner beam.

The computed value of 52 millivolts was experimentally confirmed from data recorded at sea. When the outputs of all 32 beams are averaged, the resulting value is equivalent to an individual beam output to be expected from an isotropic, random noise field. The averages of several sets of data equalled approximately 52 millivolts.

APPENDIX II

SYSTEM LINEARITY

Rudnick[11] includes the necessary expressions to compute beam output power as a function of array geometry and input signal-to-noise ratio at an individual hydrophone. Output power may be expressed as

$$W = \frac{2}{\pi} \left[\sum_{i=1}^{N} \sum_{j=1}^{N} \mu_{ij}(0) + \sum_{i=1}^{N} \sum_{j=1}^{N} c_{ij}(0) \right] \tag{1}$$

with the summations to be completed over the N array elements. The quantity, $\mu_{ij}(0)$, is the combined autocorrelation function of signal and noise. For purposes of this analysis, the spectra of signal-to-noise may be considered identical and are assigned different nomenclature only to differentiate between that noise which is within the main lobe of the directed beam and that which is outside the lobe. Implicit in the last statement is the assumption that noise is completely uncorrelated with respect to angle of arrival. $c_{ij}(0)$ is the autocorrelation function of the spectrum introduced by clipping and is defined by Rudnick[11] as

$$\frac{2}{\pi} \left[\sin^{-1} \mu_{ij}(\tau) \right] = \frac{2}{\pi} \left[\mu_{ij}(\tau) + c_{ij}(\tau) \right] \tag{2}$$

$\mu_{ij}(0)$ may be expanded to

$$\mu_{ij}(0) = \frac{n}{n+s} \rho_{ij}(0) + \frac{s}{n+s} \sigma_{ij}(0) \tag{3}$$

where ρ and σ are noise and signal autocorrelation functions respectively. $\sigma_{ij}(0) = 1$ since by definition it is the signal to which the beam is steered. $\sum_{i=1}^{N}\sum_{j=1}^{N} c_{ij}(0)$ may also be separated into

$$\sum_{i=1}^{N}\sum_{j=1}^{N} c_{ij}(0) = \sum_{i=1}^{N} c_{ii}(0) + \sum\sum_{i \neq j}^{N(N-1)} c_{i \neq j}(0) \qquad (4)$$

It follows from (2) that $c_{ii} = \pi/2 - 1$. In addition, Rudnick has shown that

$$\sum\sum_{i \neq j}^{N\ N} c_{ij}(0)$$

is small and may be neglected.

Substituting the several expressions described above into (1) and reducing terms, the output voltage of the linear half-wave rectifier can be shown to be proportional to

$$V \sim \left(\frac{N}{2\pi}\right)^{1/2} \left[1 + \frac{2}{\pi}\ \frac{n}{n+s}\ e + \frac{2}{\pi}\ \frac{s}{n+s}\ (N+1)\right]^{1/2} \qquad (5)$$

If a small signal-to-noise ratio input of s/n equal to 0.1 is assumed and with N equal to 32 and "e" equal to 0.25, equation (5) yields the value 3.87. Entering the detector characteristic of Fig. 11 with the above value, an output voltage of 90 millivolts is obtained. No recorded data was used in the analysis where the output of any beam exceeded 90 millivolts. It is concluded, therefore, that the system was operated throughout its linear region during the tests.

APPENDIX III

DERIVATION OF THE MATRIX APPROXIMATION

Considering the case of azimuthal symmetry, the output of any vertical beam may be written:

$$Y_i = \int_{4\pi} X(\theta)\, G_i\, (\theta, \phi)\, d\Omega \qquad (1)$$

where Y_i = output of i^{th} beam

X = continuous true field distribution (power/unit receiving area/unit solid angle subtended by the source)

G = power response of i^{th} beam

If the true field is assumed to be isotropic, then

$$Y_i = X_\Omega \int_{4\pi} G_i\, (\theta, \phi)\, d\Omega \qquad (2)$$

The directivity ratio of an array is defined as:

$$D.R. = \frac{\int_{4\pi} G_i\, (\theta, \phi)\, d\Omega}{G_i\, (\theta, \phi) \int_{4\pi} d\Omega} \qquad (3)$$

Combining equations (2) and (3)

$$Y_i = X_\Omega\, G\, (\theta_i, \phi_i)\, D.R.\, 4\pi \qquad (4)$$

where $G\, (\theta_i, \phi_i)$ equals unity and 0.853 for outer and inner beams respectively as defined by paragraph 2.6. Setting $4\pi X_\Omega = 1$ which has the physical interpretation of total power from all directions normalized to unity, then

$$Y_1 = \frac{\text{D.R. (outer beam)}}{0.853 \text{ D.R. (inner beam)}} \tag{5}$$

Rewriting equation (1) as a sum of eight terms, with each term representing the contribution from a spherical zone formed by two planes parallel to the equator and each zone containing one of the eight vertical beams, then:

$$Y_1 = \sum_{j=1}^{j=8} X_j \int_{\text{zone}} \sin\theta d\theta \int_0^{2\pi} G_1(\theta, \phi)\, d\phi \tag{6}$$

The true field, X_j , may be non-isotropic, although X_j is a constant within a particular zone. The quantity $G_1(\theta, \phi)$ may next be averaged over all azimuth.

$$Y_i = \sum_{j=1}^{j=8} X_j \int_{\theta_{j1}}^{\theta_{j2}} 2\pi\, \overline{G_1(\theta)}\, \sin\theta d\theta \tag{7}$$

where θ_{j1} and θ_{j2} are the limits of the spherical zones. There exists between the limits of each zone a particular value of $\theta = \theta_{\text{int}}$ which permits equation (7) to be transformed to the following

$$Y_1 = \sum_{j=1}^{j=8} X_j 2\pi\, \overline{G_1(\theta_{\text{int}})} \int_{\theta_{j1}}^{\theta_{j2}} \sin\theta d\theta \tag{8}$$

Equation (8) may be further simplified by replacing the integral by a constant, k_j , for a particular zone yielding

$$Y_i = 2\pi\, \overline{G_1(\theta_{\text{int}})} \sum_{j=1}^{j=8} k_j X_j \tag{9}$$

or more briefly

$$Y_i = a_{ij} \quad X_j \qquad\qquad i, j = 1 \rightarrow 8 \qquad\qquad (10)$$

Equation (10) relates the measured field values, Y_i , to a set of eight simultaneous equations in eight unknowns which are the true field values, X_j .

The a_{ij} matrix which satisfies equations (5) and (9) was determined by trial and error. The matrix was then inverted by digital computer to produce a set of equations of the form

$$X_j = a_{ij}^{-1} \quad Y_i$$

The coefficients of the inverted matrix are listed below. By multiplying each element of row one by Y_1 , row two by Y_2 , etc., the sum of all column one elements yields X_1 , the column two elements X_2, etc. The values of X so derived are the first approximation to the true field in the restoration process.

Table of Coefficients a_{ij}

ij	1	2	3	4	5	6	7	8
1	67.855	-32.537	27.269	-19.912	10.678	-19.322	3.122	-8.932
2	-1.677	89.327	-67.679	23.059	-19.345	16.734	-5.158	-1.845
3	-0.036	-9.622	92.536	-39.901	20.905	-32.688	0.808	-0.282
4	-1.102	2.503	-52.047	106.681	-38.812	20.422	-5.628	-0.799
5	-0.799	-5.628	20.422	-38.812	106.681	-52.047	2.503	-1.102
6	-0.282	0.808	-32.688	20.905	-39.901	92.536	-9.622	-0.036
7	-1.845	-5.158	16.734	-19.345	23.059	-67.679	89.327	-1.677
8	-8.932	3.122	-19.322	10.678	-19.912	27.269	-32.537	67.855

APPENDIX IV

TRUE FIELD RESTORATION SAMPLE COMPUTATION

In order to illustrate the restoration process, the procedures followed in deriving Fig. 18 will be described.

Table I is a random selection of recorded data typical of that which results following the film reading procedures of paragraph 3.6. The values shown are the individual beam detector outputs in millivolts following one second integration and at 14 second intervals. Beam numbering is such that beam 32 is directed at the surface, beams 27-31 at 38 degrees from the vertical, beams 22-26 at 64 degrees from the vertical, beams 17-21 at 78.5 degrees from the vertical, etc., to beam 1 directed at the bottom of the ocean. The RMS values for each beam for each run are computed and tabulated in column 2 (Aver) of Table II. The detector correction is applied (Corr Aver) and the RMS output for beams of a given colatitude computed (Vert Aver). The average of all beams is similarly determined.

Power ratios for each colatitude with respect to beam 32 and with respect to the average of all beams are computed. The Y_i column is determined by multiplying the appropriate expression of equation (5) of Appendix III by the power ratios of column 8 of Table II. The values of Y_i are then used in conjunction with the matrix of Appendix III to obtain the first approximation to the X_i .

In Fig. 24 the measured values of Y_i , expressed as decibel ratios with respect to beam 32, are plotted as dots. A faired curve connecting the first approximation values of X_i is indicated

TABLE I

Beam																			
1	51	50	51	50	51	51	51	52	50	51	51	50	50	50	51	50	51	51	50
2	49	49	49	48	48	48	49	49	48	49	48	48	49	49	48	46	47	49	49
3	47	46	46	46	47	46	47	48	47	45	46	47	47	46	46	46	46	47	47
4	49	49	48	48	49	48	48	49	49	48	49	49	49	49	49	48	49	49	49
5	50	50	49	49	50	49	50	49	49	49	49	49	50	50	49	49	50	51	49
6	47	47	47	47	47	46	47	46	45	47	47	46	46	47	46	46	47	46	47
7	49	50	49	49	49	48	49	50	49	54	51	50	50	49	50	49	50	50	50
8	50	51	50	50	49	50	50	41	50	50	50	50	51	49	50	50	51	50	50
9	48	49	49	48	49	49	50	49	48	49	49	49	49	48	48	47	40	50	48
10	49	52	50	50	50	50	51	52	50	50	50	51	50	50	50	51	51	52	50
11	46	48	47	46	47	46	48	47	48	46	47	47	48	48	47	47	48	48	46
12	42	44	43	44	45	44	45	45	45	43	44	44	45	44	44	43	44	45	43
13	42	44	45	43	43	42	44	45	44	45	44	45	43	43	43	43	44	45	44
14	41	43	43	43	43	42	44	45	43	41	42	43	42	42	42	42	43	44	43
15	46	49	49	49	49	48	49	50	48	47	49	49	49	49	48	47	48	49	47
16	50	53	54	54	54	51	53	54	53	50	54	51	52	52	52	52	51	52	52
17	47	50	49	49	49	49	49	49	48	56	52	50	50	49	50	49	49	50	49
18	54	58	51	56	56	54	57	56	56	56	57	56	56	55	55	56	56	56	54
19	48	51	51	50	50	50	51	50	50	49	49	50	51	50	49	48	50	52	49
20	50	52	51	50	51	50	51	54	52	51	50	50	49	50	51	51	50	50	51
21	54	56	51	55	57	56	55	55	53	52	54	54	55	55	53	52	53	54	51
22	50	54	51	51	51	50	52	53	54	52	52	53	52	52	52	50	52	52	51
23	64	64	64	65	64	63	63	65	64	61	66	65	66	64	60	63	63	64	63

TABLE I (CONT.)

Beam																			
24	62	62	62	61	61	61	62	61	60	59	61	62	62	60	62	59	60	63	59
25	51	53	50	51	50	50	50	52	51	50	52	51	52	51	51	51	51	51	51
26	57	59	58	58	56	54	56	59	57	56	58	57	57	58	56	57	57	60	57
27	60	59	59	60	58	58	59	58	58	56	58	58	59	59	58	57	58	60	57
28	60	59	60	61	60	59	59	59	61	58	60	61	60	58	58	57	58	62	58
29	66	62	62	63	62	64	65	64	63	62	65	66	62	62	64	60	61	65	63
30	69	74	67	65	64	64	66	65	61	64	66	69	67	68	63	64	70	63	63
31	64	63	62	64	61	64	62	66	62	60	62	64	61	65	62	62	61	61	59
32	77	78	76	74	74	76	75	77	73	74	75	76	72	74	75	76	77	75	72

[illegible]

TABLE II

Beam	Aver	Corr Aver	Vert Aver*	Elev Angle	Ratio re 32	Ratio re av.	Ratio Re 32(db)	Ratio Re av.(db)	Y_i
1	52	52	52	180°	.603	.999	-2.2	0.0	.0335
2	47	49							
3	46	48							
4	49	51	50	142°	.549	.909	-2.61	-0.42	.0287
5	48	52							
6	45	48							
7	41	40							
8	53	50							
9	48	47	47	116°	.495	.821	-3.06	-0.87	.0276
10	48	51							
11	45	47							
12	43	45							
13	41	53							
14	44	47	46	101.5°	.473	.784	-3.26	-1.06	.0248
15	47	49							
16	44	44							
17	53	55							
18	47	48							
19	45	47	52	78.5°	.611	1.010	-2.15	0.05	.0319
20	46	48							
21	61	62							
22	56	56							
23	56	52							
24	52	52	55	64°	.671	1.122	-1.74	0.46	.0376
25	53	--							
26	61	59							
27	54	58							
28	54	58							
29	--	--	60	38°	.797	1.320	-0.98	1.21	.0417
30	59	64							
31	57	59							
32	67	67	67	0°	1.000	1.655	0	2.19	.0556

*Vertical Average - The averaged output of all beams of equal elevation angle.

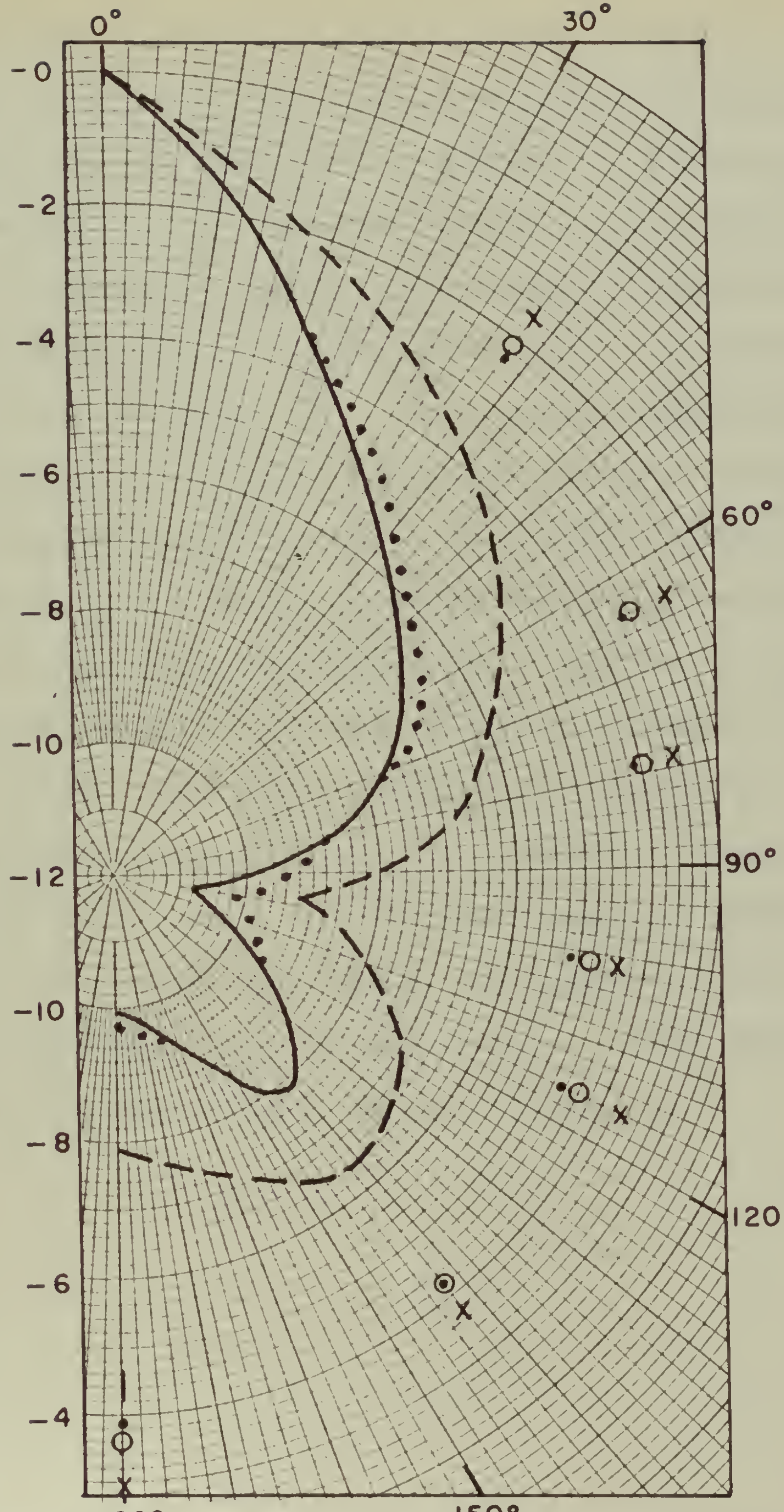

FIGURE 24 TRUE FIELD VERTICAL DISTRIBUTION
HERATIVE SOLUTION

by dashed lines. This curve is used to select values of X_i in 10 degrees steps to complete the numerical integration of equation (1) of paragraph 6.1. The integration of equation (1) was accomplished with incremental steps of 10 degrees in elevation and azimuth. Figure 25 represents the results of all computations with the exception of the integration over the variable, θ. The ordinate is $G(\theta)\ X(\theta) \sin\theta$, the abscissa, θ. The 8 curves represent the 8 vertical beams and is included to illustrate the fact that the beam response contributes significantly in all directions and emphasizes the importance to this process of knowing the beam patterns exactly. The curves of Fig. 25 are then integrated by planimeter and the decibel ratios between a given beam and the beam directed at the surface obtained. The results are plotted as X's in Fig. 24. The decibel difference between dots and X's is measured and twice that value applied as a correction to the first assumption, dashed curve, of Fig. 24. The dotted curve results. The numerical integration process is repeated yielding the open circles. A final iteration yields the solid curve which is the curve of Fig. 18.

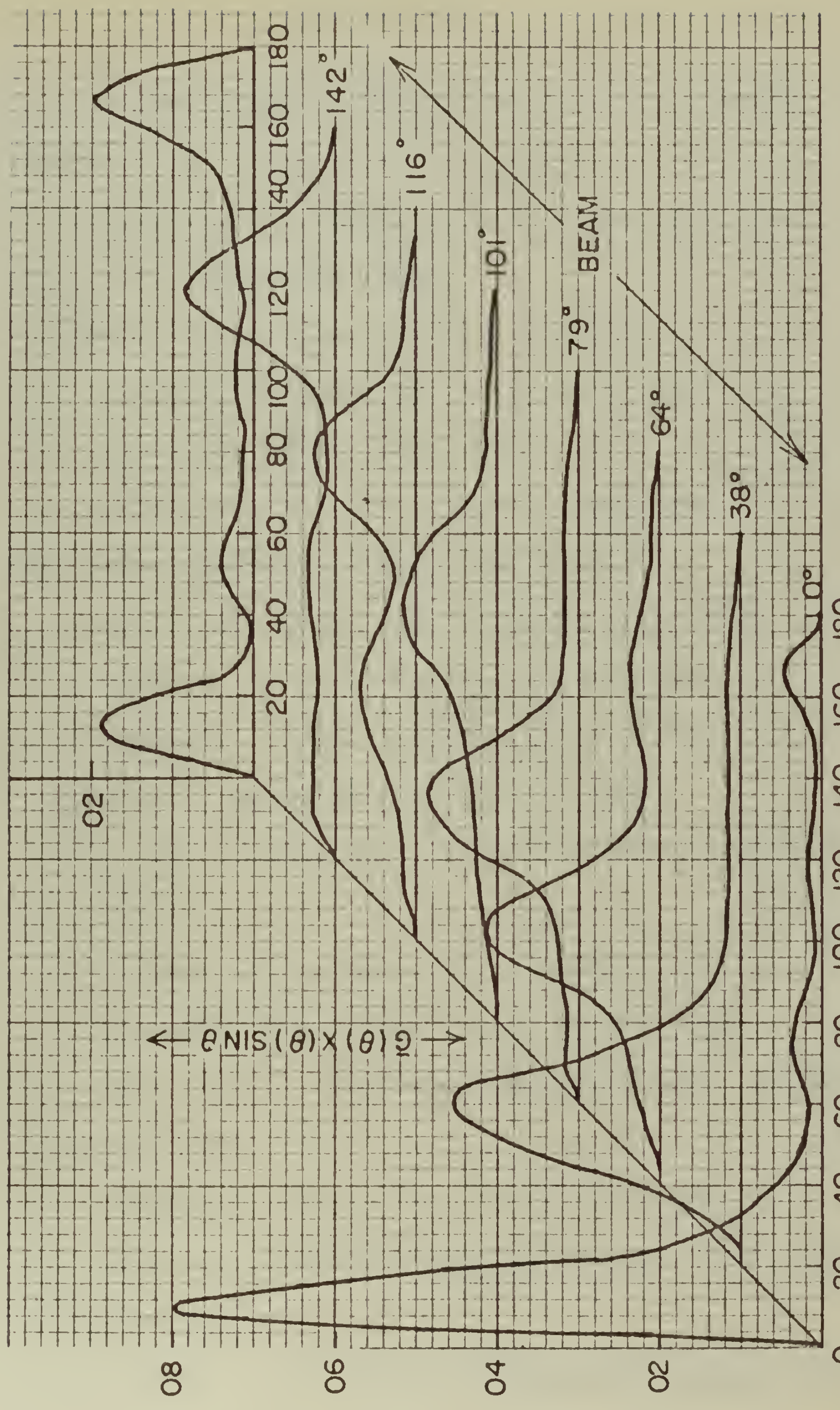

FIGURE 25. G(θ)X(θ)SIN θ VS θ

BIBLIOGRAPHY

1. R. A. Frosch, Unpublished paper, Acous. Soc. Am. Meeting, June (1960).
2. V. O. Knudsen, R. S. Alford and J. W. Emling, Rpt. No. 3, NDRC Sec. No. 6. 1-NDRC-1848 (1944).
3. C. Eckart, J. Acous. Soc. Am. 25, 195 (1953).
4. R. E. Roberson, J. Acous. Soc. Am. 25, 353 (1951).
5. R. J. Urick, NRL Report 3769 (1951).
6. C. N. Miller, NEL Conf. Rpt. 698 of 22 June 1956.
7. NRDC Summary Technical Reports, Div. 6, 8.
8. C. A. Teer, Great Britain UDE Report No. 65, (1949).
9. V. C. Anderson, J. Acous. Soc. Am. 30, 440 (1958).
10. V. C. Anderson, J. Acous. Soc. Am. 32, 867 (1960).
11. P. Rudnick, J. Acous. Soc. Am. 32, 871 (1960).
12. H. Primakoff, Columbia Div. of War Res. Library of Congress No. L3363
13. V. C. Anderson MPL Tech Memo 112, 26 January 1960.
14. R. N. Bracewell, Aust. Jour. of Phys. 7, 615 (1954).
15. T. G. Bell, Paper to 18th Underwater Acous. Symp., Monterey, 25 October 1960.
16. K. V. MacKenzie, J. Acous. Soc. Am. 32, 221 (1960).
17. H. W. Marsh and M. Schulkin, USL Tech Memo No. 1110-110-54 27 August 1954.
18. J. L. Lawson and G. E. Uhlenbeck, "Threshold Signals," McGraw-Hill, M.I.T. Radiation Laboratory Series, Vol. 24.